

# Fluorescent Non-peptidic RGD Mimetics with High Selectivity for $\alpha_v\beta_3$ vs $\alpha_{IIb}\beta_3$ Integrin Receptor: Novel Probes for in Vivo Optical Imaging

Wael Alsibai,<sup>†</sup> Anke Hahnenkamp,<sup>†</sup> Michel Eisenblätter,<sup>†,§</sup> Burkhard Riemann,<sup>‡</sup> Michael Schäfers,<sup>||,⊥,‡</sup> Christoph Bremer,<sup>⊥,○</sup> Günter Haufe,<sup>⊥,#</sup> and Carsten Hölteke<sup>\*,†</sup>

<sup>†</sup>Department of Clinical Radiology, <sup>‡</sup>Department of Nuclear Medicine, University Hospital Muenster, Muenster D-48149, Germany

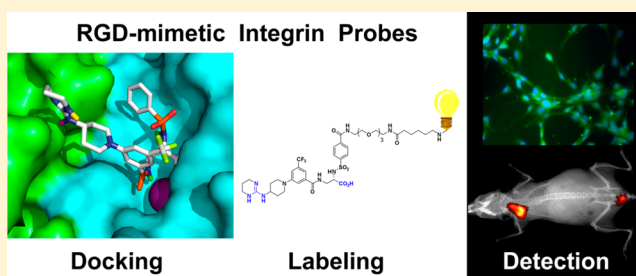
<sup>§</sup>Division of Imaging Sciences, King's College London, London SE1 7EH, United Kingdom

<sup>||</sup>European Institute for Molecular Imaging (EIMI), <sup>⊥</sup>Cluster of Excellence DFG EXC 1003 "Cells-in-Motion—CiM",

<sup>#</sup>Organic Chemistry Institute, University of Muenster, Muenster D-48149, Germany

<sup>○</sup>Clinic for Radiology, St. Franziskus Hospital Muenster, Muenster D-48145, Germany

**ABSTRACT:** Integrins are heterodimeric transmembrane protein receptors consisting of different  $\alpha$  and  $\beta$  subunits.  $\alpha_v\beta_3$  integrins are overexpressed on many tumor cells and tumor-associated angiogenic vessels, whereas  $\alpha_{IIb}\beta_3$  is a receptor for, e.g., fibrinogen and mediates platelet aggregation. In this study, a near-infrared fluorescent imaging probe has been designed and synthesized by conjugating fluorescent dyes to a non-peptidic, pharmacophore-based ligand, based on a molecular modeling design approach. Affinity values were determined, and in vitro cell binding assays and preliminary in vivo xenograft studies in nude mice were performed to evaluate target binding. Competition assays revealed excellent binding and selectivity to  $\alpha_v\beta_3$  compared to that for  $\alpha_{IIb}\beta_3$ . In vitro, the probe showed high target binding on  $\alpha_v\beta_3$ -positive M-21 cells and negligible binding to  $\alpha_v\beta_3$ -negative MCF-7 cells. In vivo, the tracer is able to image target expression in U-87 xenografts with a maximum signal-to-noise ratio (SNR) of 2.5:1 at 24 h after injection.



## INTRODUCTION

Integrins are a large family of cell adhesion molecules consisting of one  $\alpha$  and one  $\beta$  subunit. To date, more than 20 of these heterodimeric transmembrane receptors are known. They function as cell adhesion mediators and signal transduction platforms in a large variety of (patho)physiological processes, including immune response, platelet aggregation, and cell migration and proliferation.<sup>1–5</sup> The  $\alpha_{IIb}\beta_3$  integrin is mainly located on platelets, where it comprises about 80% of the proteins expressed on the surface. On activation, it is responsible for platelet aggregation and, finally, thrombus formation.<sup>6,7</sup> Integrin  $\alpha_v\beta_3$  is known to be highly expressed on the surface of angiogenic endothelial cells and a variety of solid tumors. In particular, pathophysiological angiogenic processes are mediated by  $\alpha_v\beta_3$ . Besides  $\alpha_v\beta_3$  and  $\alpha_{IIb}\beta_3$ , a large number of other integrins bind ligands via an Arg-Gly-Asp (RGD) amino acid motif. Ligands include fibronectin, fibrinogen, vitronectin, von Willebrand factor, laminin, and others.<sup>3,8</sup> One common element of these ligands is the Asp carboxylic acid function, which coordinates to the bivalent cation at the metal ion-dependent adhesion site (MIDAS) of the  $\beta$ -subunit.<sup>1</sup> The in vivo imaging of integrins, especially  $\alpha_v\beta_3$  as a potential marker for angiogenic activity, has become very prominent due to the availability of small peptides with the RGD motif.<sup>9–13</sup> Molecular imaging of  $\alpha_v\beta_3$  expression could potentially aid in the evaluation of tumor-related

angiogenesis (e.g., as a surrogate for tumor aggressiveness) and facilitate the assessment of therapy response to antiangiogenic drugs (e.g., Bevacizumab).<sup>14</sup> Recently, for diagnostic as well as for therapeutic purposes, non-peptidic RGD mimetic compounds have become available. Tirofiban, a selective  $\alpha_{IIb}\beta_3$  inhibitor, is approved for use in percutaneous coronary intervention and in acute coronary syndromes for thrombosis prevention.<sup>15,16</sup> MK-0429, a potent  $\alpha_v\beta_3$  antagonist, is undergoing clinical trials for prostate cancer patients.<sup>17</sup> The affinity of ligands to  $\alpha_{IIb}\beta_3$  would be potentially detrimental, especially for therapeutic purposes targeting other integrins, because of its involvement in platelet aggregation and thrombus formation. Therefore, the selectivity of antagonists for, e.g.,  $\alpha_v\beta_3$  is of great importance.<sup>8</sup> On the basis of a recently published lead structure (5, Figure 1),<sup>18</sup> we present here the synthesis of a fluorescent integrin probe with high specificity and selectivity, which may facilitate the assessment of  $\alpha_v\beta_3$  integrin expression in vivo by means of near-infrared optical imaging.

## MATERIALS AND METHODS

**General.** All chemicals, reagents, and solvents used for the synthesis of compounds were analytical grade and purchased from

Received: August 5, 2014

commercial sources. Sulfobenzoic acid monopotassium salts (**12a** and **12b**) and (S)-2,3-diaminopropanoic acid (DAP) were from Sigma-Aldrich (Schnelldorf, Germany). The poly(ethylene glycol) (PEG) derivatives 2-(2-(2-(2-azidoethoxy)ethoxy)ethoxy)ethylamine ( $\text{NH}_2\text{-PEG}_4\text{-N}_3$ ) and 2-(2-(2-(2-azidoethoxy)ethoxy)ethoxy)ethylmethanesulfonate ( $\text{MsO-PEG}_4\text{-N}_3$ ) were synthesized according to recently described procedures.<sup>19</sup> Lead compound **5** was synthesized as shown in Scheme 1 and reported in the literature.<sup>18</sup> The RGD peptide used for blocking studies (*cyclo*-[CRGDC]GK) was purchased from Bachem (Bubendorf, Switzerland) and has been used before.<sup>20,21</sup> Nuclear magnetic resonance (NMR) spectra ( $^1\text{H}$ ,  $^{13}\text{C}$  and  $^{19}\text{F}$ ) were recorded on a Bruker AV 300 or AV 400 instrument (Bruker BioSpin GmbH, Rheinstetten, Germany) or an Agilent DD2 600 instrument (Agilent Technologies Deutschland GmbH, Boeblingen, Germany), respectively. Mass spectrometry (MS) was performed using a Bruker MALDI-TOF-MS Reflex IV (matrix: DHB, Bruker Daltonics GmbH, Bremen, Germany) or a Waters QUATTRO LCZ (high-resolution mass spectrometry, HRMS, Waters Micromass, Manchester, UK) spectrometer with a nanospray capillary inlet. High-pressure liquid chromatography (HPLC) analysis and purification was performed on a gradient reversed-phase (RP)-HPLC using a Knauer system with two K-1800 pumps, an S-2500 UV detector (Herbert Knauer GmbH, Berlin, Germany), and RP-HPLC Nucleosil 100-5 C18 columns (250 mm  $\times$  8.0 mm and 250 mm  $\times$  20 mm). The recorded data was processed by ChromGate HPLC software (Knauer). Unless otherwise mentioned, the purity of the synthesized compounds was determined with the same HPLC system and Nucleosil 100-5 C18 column (250 mm  $\times$  8.0 mm). All compounds tested had  $\geq 95\%$  purity.

**Docking Studies.** Docking studies were performed with the AutoDock Vina software tool using default parameters. The crystal structure 1L5G from the Research Collaboratory for Structural Bioinformatics (RCSB) Protein Data Bank was chosen. The co-crystallization RGD peptide and water molecules were subtracted using AutoDock Tools, and hydrogen atoms were added or subtracted at polar amino acid sites. In addition, the  $\text{Mn}^{2+}$  atom at the MIDAS in the  $\alpha,\beta_3$  crystal structure was replaced with  $\text{Mg}^{2+}$ . The 3D structure of parent compound **5** was constructed using ChemDraw Ultra 12.0 together with the MM2 force-field method from Chem3D. Degrees of freedom and rotatable bonds were defined by AutoDock Tools software.<sup>22</sup> The binding pocket was placed inside a grid ( $x = 16$ ,  $y = 42$ ,  $z = 41$ ) with a size of  $45 \times 45 \times 45 \text{ \AA}^3$  and a distance of points of 1  $\text{\AA}$ . The evaluation of the docking results and the visualization were performed using PyMOL 1.3 viewer software.

**Synthetic Methods.** 4-(Benzyloxy)benzenesulfonic Acid (**7**). Monosodium-4-hydroxybenzenesulfonic acid dihydrate (**6**) (20.0 g, 86.1 mmol) was dissolved in 200 mL of DMF, and NaH (60%, 4.13 g, 103.4 mmol) was added. The mixture was cooled to  $-10^\circ\text{C}$ , and benzyl bromide (12.3 mL, 103.4 mmol) was added under vigorous stirring. After stirring for 6 h at room temperature (rt), the reaction was quenched by the addition of ethyl acetate (20 mL). The suspension was filtered, and the residue was washed twice with ethyl acetate. The solvent was evaporated, and the residue was recrystallized from ethyl acetate, yielding 22.8 g (86 mmol, 93%) of a colorless solid. mp  $93\text{--}94^\circ\text{C}$ .  $^1\text{H}$  NMR (300 MHz, DMSO- $d_6$ )  $\delta$  7.63–7.20 (m, 7H), 6.95–6.89 (m, 2H), 5.10 (s, 2H).  $^{13}\text{C}$  NMR (75 MHz, DMSO- $d_6$ )  $\delta$  158.8, 141.6, 137.4, 128.9, 128.2, 128.1, 127.5, 114.1, 69.6. Corresponding spectroscopic data can also be found in the literature.<sup>23</sup> HRMS (ESI $^+$ ):  $\text{C}_{13}\text{H}_{12}\text{O}_4\text{S} - \text{H}^+$  calcd, 263.0373; found, 263.0382.

4-(Benzyloxy)benzene-1-sulfonyl Chloride (**8**). A solution of 4-(benzyloxy)benzenesulfonic acid (22.0 g, 83 mmol) in dimethylformamide (DMF, 150 mL) was treated with thionylchlorid (6.6 mL, 90.0 mmol) at  $0^\circ\text{C}$  and then stirred for 2 h at rt. The mixture was carefully diluted with water and then extracted with methylene chloride. The combined extracts were dried over  $\text{MgSO}_4$ , filtered, and evaporated to give 22.8 g (80 mmol, 97%) of a light-brown solid.  $^1\text{H}$  NMR (300 MHz,  $\text{CDCl}_3$ )  $\delta$  8.03–7.96 (m, 2H), 7.52–7.34 (m, 5H), 7.19–7.08 (m, 2H), 5.19 (s, 2H).  $^{13}\text{C}$  NMR (75 MHz,  $\text{CDCl}_3$ )  $\delta$  163.9, 136.3, 135.2, 129.6, 128.9, 128.6, 127.5, 115.5, 70.7. Corresponding spectroscopic data can also be found in the literature.<sup>23</sup>

Methyl-(S)-2-Amino-3-[(*tert*-butoxycarbonyl)amino]propanoate (**9**). (S)-2,3-Diaminopropanoic acid (DAP, 10.0 g, 71.4 mmol) was converted to its methyl ester by treatment with thionyl chloride (170 mL) in methanol (300 mL) at reflux for 48 h. After evaporation and azeotropic distillation of excess thionyl chloride with toluene, the product dihydrochloride remained as a colorless solid in 96% yield (13.0 g, 68.4 mmol).  $^1\text{H}$  NMR (400 MHz, DMSO- $d_6$ )  $\delta$  8.96 (s, 6H,  $\text{NH}_2$ ), 4.44 (t,  $^3J_{\text{H-H}} = 5.9 \text{ Hz}$ , 1H), 3.73 (s, 3H), 3.40–3.26 (m, 2H).  $^{13}\text{C}$  NMR (101 MHz, DMSO- $d_6$ )  $\delta$  166.9, 53.4, 49.9, 38.2. Subsequent Boc (*tert*-butoxycarbonyl)-protection at the  $\alpha$ -position was possible by treatment of the above dihydrochloride (10.0 g, 52.6 mmol) with 0.9 equiv of  $\text{Boc}_2\text{O}$  (10.4 g, 0.48 mmol) and triethylamine (30 mL, 2.00 mmol) in methylene chloride (800 mL) at low temperature ( $-78^\circ\text{C}$ ). The desired monoprotected product (**5**) was obtained in 53% yield (4.32 g) after chromatographic purification (2.5% methanol/ethyl acetate).  $^1\text{H}$  NMR (300 MHz,  $\text{CDCl}_3$ )  $\delta$  5.11 (s, 1H, NH), 3.71 (s, 3H), 3.60–3.46 (m, 2H), 3.31–3.15 (m, 1H), 1.64 (s, 2H,  $\text{NH}_2$ ), 1.42 (s, 9H).  $^{13}\text{C}$  NMR (75 MHz,  $\text{CDCl}_3$ )  $\delta$  174.5, 155.9, 79.5, 54.4, 52.3, 44.2, 28.3. GC-MS  $m/z$  (%): 162 (11), 145 (13), 130 (9), 103 (22), 101 (20), 89 (50), 88 (43), 74 (26), 57 (100), 41 (63). HRMS:  $\text{C}_9\text{H}_{18}\text{N}_2\text{O}_4 + \text{H}^+$  calcd, 219.1339; found, 219.1324;  $\text{C}_9\text{H}_{18}\text{N}_2\text{O}_4 + \text{Na}^+$  calcd, 241.1159; found, 241.1143.

Methyl-(S)-2-[4-(Benzyloxy)phenylsulfonamido]-3-[(*tert*-butoxycarbonyl)amino]propanoate (**10**). Methyl-(S)-2-amino-3-[(*tert*-butoxycarbonyl)amino]propanoate (**9**) (2.01 g, 9.2 mmol) was dissolved in methylene chloride and treated with triethylamine (4.5 mL, 37 mmol) and 4-(benzyloxy)benzene-1-sulfonyl chloride (**8**) (2.60 g, 9.2 mmol) at  $0^\circ\text{C}$ . After stirring overnight at rt, the mixture was diluted with water and extracted with methylene chloride. The combined extracts were dried over  $\text{MgSO}_4$ , filtered, and evaporated to give the raw product, which was purified by column chromatography (cyclohexane/ethyl acetate, 2:1). Yield: 3.2 g (6.9 mmol, 93%).  $^1\text{H}$  NMR (300 MHz,  $\text{CDCl}_3$ )  $\delta$  7.87–7.65 (m, 2H), 7.53–7.29 (m, 5H), 7.08–6.94 (m, 2H), 5.46 (d,  $^3J_{\text{H-H}} = 7.8 \text{ Hz}$ , 1H, NH), 5.12 (s, 2H), 4.90 (s, 1H, NH), 3.94 (dt,  $^3J_{\text{H-H}} = 7.8 \text{ Hz}$ ,  $^3J_{\text{H-H}} = 4.9 \text{ Hz}$ , 1H), 3.55 (s, 3H), 3.52–3.34 (m, 2H), 1.42 (s, 9H).  $^{13}\text{C}$  NMR (75 MHz,  $\text{CDCl}_3$ )  $\delta$  170.3, 162.2, 155.9, 135.0, 131.0, 129.4, 128.8, 128.4, 127.5, 115.2, 77.2, 70.3, 55.9, 52.1, 43.2, 28.2. HRMS (ESI $^+$ ):  $\text{C}_{22}\text{H}_{28}\text{N}_2\text{O}_7\text{S} + \text{Na}^+$  calcd, 487.1509; found, 487.1507;  $(\text{C}_{22}\text{H}_{28}\text{N}_2\text{O}_7\text{S})_2 + \text{Na}^+$  calcd, 951.3127; found, 951.3151.

Methyl-2-[4-(2-[2-(2-azidoethoxy)ethoxy]ethoxy)ethoxy]phenylsulfonamido]-3-[(*tert*-butoxycarbonyl)amino]propanoate (**11**). Methyl-(S)-2-[4-(benzyloxy)phenylsulfonamido]-3-[(*tert*-butoxycarbonyl)amino]propanoate (**10**) (3.0 g, 6.9 mmol) was dissolved in 40 mL of a 1:1 mixture of methanol and 1,4-dioxane in a hydrogenation apparatus, and  $\text{Pd}(\text{OH})_2$  (10% w/w) was added. Hydrogenolysis of the benzyl protecting group was performed at a hydrogen pressure of 40 atm. After filtration and evaporation the deprotected product, methyl (S)-2-(4-hydroxyphenylsulfonamido)-3-[(*tert*-butoxycarbonyl)amino]propanoate was isolated as a colorless powder. Yield: 2.5 g (6.9 mmol, 98%), mp  $80.2^\circ\text{C}$  (recrystallized from methanol).  $^1\text{H}$  NMR (400 MHz,  $\text{CDCl}_3$ )  $\delta$  7.69 (d,  $^3J_{\text{H-H}} = 8.8 \text{ Hz}$ , 2H), 6.90 (d,  $^3J_{\text{H-H}} = 8.8 \text{ Hz}$ , 2H), 5.59 (d,  $^3J_{\text{H-H}} = 8.1 \text{ Hz}$ , 1H), 5.05 (s, 1H), 3.96 (dt,  $^3J_{\text{H-H}} = 7.5 \text{ Hz}$ ,  $^3J_{\text{H-H}} = 5.1 \text{ Hz}$ , 1H), 3.57 (s, 3H), 3.49–3.40 (m, 2H), 1.79 (s, 1H), 1.43 (s, 9H).  $^{13}\text{C}$  NMR (101 MHz,  $\text{CDCl}_3$ )  $\delta$  170.4, 160.4, 156.2, 130.2, 129.6, 115.9, 80.4, 55.8, 53.1 (q, C-5), 43.2 (t, C-8), 28.3 (q, C-11). HRMS (ESI $^+$ ):  $\text{C}_{15}\text{H}_{22}\text{N}_2\text{O}_7\text{S} + \text{Na}^+$  calcd, 397.1040; found, 397.1039;  $(\text{C}_{15}\text{H}_{22}\text{N}_2\text{O}_7\text{S})_2 + \text{Na}^+$  calcd, 771.2182; found, 771.2172.

The above methyl (S)-2-(4-hydroxyphenylsulfonamido)-3-[(*tert*-butoxycarbonyl)amino]propanoate (2.0 g, 5.35 mmol) and 2-[2-(2-azidoethoxy)ethoxy]ethoxyethylmethanesulfonate ( $\text{MsO-PEG}_4\text{-N}_3$ ) (2.0 g, 8.03 mmol) were dissolved in DMF (15 mL) and treated with  $\text{K}_2\text{CO}_3$  (1.1 g, 8.03 mmol). The mixture was heated at  $90^\circ\text{C}$  overnight, diluted with water (40 mL), and extracted with chloroform ( $3 \times 50 \text{ mL}$ ). After drying over  $\text{MgSO}_4$  and evaporation of the solvent, **11** was purified by column chromatography (cyclohexane/ethyl acetate 2:1). Yield: 0.55 g (0.54 mmol, 10%).  $^1\text{H}$  NMR (400 MHz,  $\text{CDCl}_3$ )  $\delta$  7.66 (d,  $^3J_{\text{H-H}} = 8.8 \text{ Hz}$ , 2H), 6.90 (d,  $^3J_{\text{H-H}} = 8.8 \text{ Hz}$ , 2H), 5.22 (t,  $^3J_{\text{H-H}} = 6.1 \text{ Hz}$ , 1H), 4.26–4.19 (m, 1H), 3.97 (t,  $^3J_{\text{H-H}} = 4.9 \text{ Hz}$ , 1H),

3.80–3.60 (m, 12H), 3.55 (s, 3H), 3.45 (t,  $^3J_{\text{H-H}} = 5.5$  Hz, 2H), 3.39 (m, 2H), 1.42 (s, 9H).  $^{13}\text{C}$  NMR (101 MHz,  $\text{CDCl}_3$ )  $\delta$  170.6, 160.9, 156.5, 129.5, 116.0, 80.5, 70.0 (several signals), 69.1, 63.7, 55.8, 53.0, 50.7, 43.2, 28.3. HRMS (ESI<sup>+</sup>):  $\text{C}_{23}\text{H}_{37}\text{N}_3\text{O}_{10}\text{S} + \text{H}^+$  calcd, 576.2334; found, 576.2339;  $\text{C}_{23}\text{H}_{37}\text{N}_3\text{O}_{10}\text{S} + \text{Na}^+$  calcd, 598.2154; found, 598.2160. Anal. Calcd: C, 50.27; H, 6.19; N, 7.82. Found: C, 50.27; H, 6.11; N, 7.66.

**3- and 4-(Chlorosulfonyl)benzoyl Chloride (13a,b).** The bis-chlorination of monopotassium sulfobenzoic acids **12a** and **12b** was accomplished by treating the solid salts with an excess of freshly distilled thionyl chloride and a catalytic amount of DMF at reflux under argon. In detail, from 1.80 g (4.20 mmol) of **12a** and 20 mL of thionyl chloride containing 100  $\mu\text{L}$  of DMF, after filtration, evaporation, and azeotropic distillation with toluene, product **13a** was obtained as a colorless solid in a yield of 97% (0.96 g, 4.01 mmol). From 2.70 g (6.30 mmol) of **12b** and 30 mL of thionyl chloride containing 150  $\mu\text{L}$  of DMF, **13b** was obtained and as a colorless oil in a yield of 98% (1.50 g, 6.28 mmol). **13a**:  $^1\text{H}$  NMR (300 MHz,  $\text{CDCl}_3$ )  $\delta$  8.40–8.34 (m, 2H), 8.25–8.18 (m, 2H).  $^{13}\text{C}$  NMR (75 MHz,  $\text{CDCl}_3$ )  $\delta$  167.0, 148.9, 138.5, 132.2, 127.5. **13b**:  $^1\text{H}$  NMR (300 MHz,  $\text{CDCl}_3$ )  $\delta$  8.77 (t,  $^3J_{\text{H-H}} = 1.8$  Hz, 1H), 8.49 (ddd,  $^3J_{\text{H-H}} = 7.9$  Hz,  $^4J_{\text{H-H}} = 1.7$  Hz,  $^5J_{\text{H-H}} = 1.1$  Hz, 1H), 8.36 (ddd,  $^3J_{\text{H-H}} = 8.0$  Hz,  $^4J_{\text{H-H}} = 1.9$  Hz,  $^5J_{\text{H-H}} = 1.1$  Hz, 1H), 7.85 (t,  $^3J_{\text{H-H}} = 8.0$  Hz, 1H).  $^{13}\text{C}$  NMR (75 MHz,  $\text{CDCl}_3$ )  $\delta$  166.5, 145.4, 136.9, 134.9, 132.8, 130.8, 129.4. GC-MS  $m/z$  (%): 203 (100), 175 (9), 139 (15), 104 (16), 76 (29), 50 (20).

**3- and 4-[(2-{2-[2-(2-Azidoethoxy)ethoxy]ethoxy}ethyl)-carbamoyl]benzene-1-sulfonyl Chloride (14a,b).** The chlorosulfonylbenzoyl chlorides **13a** and **13b** were treated with 2-{2-[2-(2-Azidoethoxy)ethoxy]ethoxy}ethylamine (0.9 equiv) and triethylamine (0.9 equiv) in tetrahydrofuran (THF) at  $-78^\circ\text{C}$  via addition of catalytic amounts of dimethylaminopyridine (DMAP). In detail, from 3.00 g (12.5 mmol) of **13a** and 2.61 g (11.9 mmol) of the amine in 70 mL of THF containing 1.20 g (11.8 mmol) of triethylamine, the carboxy-amide **14a** was obtained after chromatographic purification (cyclohexane/diethyl ether 1:1) in a yield of 72% (3.60 g, 8.57 mmol). From 4.00 g (16.7 mmol) of **13b** and 3.30 g (15.0 mmol) of amine in 70 mL of THF containing 1.50 g (15.0 mmol) of triethylamine, the carboxy-amide **14b** was obtained after chromatographic purification (cyclohexane/diethyl ether 1:1) in a yield of 61% (4.20 g, 10.7 mmol). **14a**:  $^1\text{H}$  NMR (300 MHz,  $\text{CDCl}_3$ )  $\delta$  8.30–8.19 (m, 4H), 7.13 (s, 1H, NH), 3.82–3.58 (m, 14H), 3.35 (t,  $^3J_{\text{H-H}} = 5.0$  Hz, 2H).  $^{13}\text{C}$  NMR (75 MHz,  $\text{CDCl}_3$ )  $\delta$  165.2, 146.1, 140.8, 128.6, 127.2, 70.6, 70.4, 70.2, 69.9, 69.4 (2 signals), 50.6, 40.1. HRMS:  $\text{C}_{15}\text{H}_{21}\text{ClN}_4\text{O}_6\text{S} + \text{H}^+$  calcd, 421.0951; found, 421.0949;  $\text{C}_{15}\text{H}_{21}\text{ClN}_4\text{O}_6\text{S} + \text{Na}^+$  calcd, 443.0770; found, 443.0767. **14b**:  $^1\text{H}$  NMR (300 MHz,  $\text{CDCl}_3$ )  $\delta$  8.49 (t,  $^3J_{\text{H-H}} = 1.8$  Hz, 1H), 8.28–8.22 (m, 1H), 8.16 (ddd,  $^3J_{\text{H-H}} = 8.0$  Hz,  $^4J_{\text{H-H}} = 1.8$  Hz,  $^5J_{\text{H-H}} = 1.1$  Hz, 1H), 7.73 (t,  $^3J_{\text{H-H}} = 7.9$  Hz, 1H), 7.28 (s, 1H, NH), 3.75–3.60 (m, 14H), 3.36 (t,  $^3J_{\text{H-H}} = 5.0$  Hz, 2H).  $^{13}\text{C}$  NMR (75 MHz,  $\text{CDCl}_3$ )  $\delta$  164.8, 144.5, 136.4, 134.1, 130.1, 129.3, 125.5, 70.6, 70.6, 70.4, 70.2, 69.9, 69.5, 50.6, 40.2. HRMS:  $\text{C}_{15}\text{H}_{21}\text{ClN}_4\text{O}_6\text{S} + \text{Na}^+$  calcd, 443.0770; found, 443.0767.

**(S)-Methyl-N-alpha-arylsulfonamide-diaminopropionates (15a,b).** The PEGylated sulfonyl chlorides **14a** and **14b** were treated with **9** to yield after deprotection the (S)-methyl-3-amino-2-(4-[(2-{2-[2-(2-azidoethoxy)ethoxy]ethoxy}ethyl)carbamoyl]phenylsulfonamido)-propanoates **15a** and **15b**. In detail, 1 equiv of **9** (0.93 g, 4.26 mmol) and 1.2 equiv of triethylamine (710  $\mu\text{L}$ , 5.11 mmol) were diluted in methylene chloride and cooled to  $0^\circ\text{C}$ . After addition of 1.1 equiv of **14a** or **14b** (1.96 g, 4.69 mmol), respectively, the mixtures were stirred for 5 h at rt followed by aqueous workup. Purification by column chromatography (cyclohexane/ethyl acetate 1:1) gave the Boc-protected derivatives in 93 and 73% yield, respectively.  $^1\text{H}$  NMR (400 MHz,  $\text{CDCl}_3$ )  $\delta$  7.98–7.84 (m, 4H), 5.75 (s, 1H, NH), 4.99 (s, 1H, NH), 4.10–3.92 (m, 1H), 3.78–3.61 (m, 14H), 3.57–3.61 (m, 3H), 3.54–3.41 (m, 2H), 3.36 (t,  $^3J_{\text{H-H}} = 5.0$  Hz, 2H), 1.95 (s, 1H, NH), 1.54–1.34 (m, 9H).  $^{13}\text{C}$  NMR (101 MHz,  $\text{CDCl}_3$ )  $\delta$  170.1, 165.8, 156.1, 142.1, 138.7, 128.0, 127.3, 80.2, 70.7, 70.5, 70.3, 70.0 (2 signals), 69.5, 56.1, 53.0, 50.6, 43.3, 40.0, 28.2. HRMS:  $\text{C}_{24}\text{H}_{38}\text{N}_6\text{O}_{10}\text{S} + \text{Na}^+$  calcd, 625.2262; found, 625.2255;

$(\text{C}_{24}\text{H}_{38}\text{N}_6\text{O}_{10}\text{S})_2 + \text{Na}^+$  calcd, 1227.4611; found, 1227.4600.  $^1\text{H}$  NMR (400 MHz,  $\text{CDCl}_3$ )  $\delta$  8.27 (s, 1H), 8.09 (d,  $^3J_{\text{H-H}} = 7.8$  Hz, 1H), 7.96 (ddd,  $^3J_{\text{H-H}} = 7.8$  Hz,  $^4J_{\text{H-H}} = 1.7$  Hz,  $^5J_{\text{H-H}} = 1.2$  Hz, 1H), 7.59 (t,  $^3J_{\text{H-H}} = 7.8$  Hz, 1H), 6.11 (s, 1H, NH), 5.12 (t,  $^3J_{\text{H-H}} = 6.4$  Hz, 1H, NH), 4.09–4.05 (m, 1H), 3.80–3.59 (m, 14H), 3.57 (s, 3H), 3.53–3.43 (m, 2H), 3.37 (t,  $^3J_{\text{H-H}} = 5.0$  Hz, 2H), 2.26 (s, 1H, NH), 1.42 (s, 9H).  $^{13}\text{C}$  NMR (101 MHz,  $\text{CDCl}_3$ )  $\delta$  171.2, 165.7, 156.1, 140.2, 135.8, 132.1, 129.5, 129.4, 125.4, 80.1, 70.6, 70.5, 70.2, 69.9 (2 signals), 69.6, 56.1, 52.9, 50.7, 43.1, 40.1, 28.3. HRMS:  $\text{C}_{24}\text{H}_{38}\text{N}_6\text{O}_{10}\text{S} + \text{H}^+$  calcd, 603.2443; found, 625.2444;  $\text{C}_{24}\text{H}_{38}\text{N}_6\text{O}_{10}\text{S} + \text{Na}^+$  calcd, 625.2262; found, 625.2255.

Subsequent deprotection of the intermediates with HCl (4 M in dioxane) gave **15a** and **15b** as monohydrochlorides in yields of 94% (**15a**, 2.00 g, 3.71 mmol) and 96% (**15b**, 1.61 g, 2.98 mmol), respectively. **15a**:  $^1\text{H}$  NMR (300 MHz,  $\text{CD}_3\text{OD}$ )  $\delta$  8.04–7.93 (m, 4H), 4.32 (dd,  $^3J_{\text{H-H}} = 9.0$  Hz,  $^3J_{\text{H-H}} = 4.9$  Hz, 1H), 3.72–3.56 (m, 16H), 3.44 (s, 3H), 3.34 (t,  $^3J_{\text{H-H}} = 4.8$  Hz, 2H), 3.29–3.33 (m, 1H), 3.10–2.93 (m, 1H).  $^{13}\text{C}$  NMR (101 MHz,  $\text{CD}_3\text{OD}$ )  $\delta$  169.4, 168.6, 143.9, 139.9, 129.2, 128.6, 71.6, 71.5, 71.3, 71.1, 70.4, 68.1, 55.0, 53.5, 51.8, 42.1, 41.1. HRMS:  $\text{C}_{19}\text{H}_{30}\text{N}_6\text{O}_8\text{S} + \text{H}^+$  calcd, 503.1919; found, 503.1927;  $\text{C}_{19}\text{H}_{30}\text{N}_6\text{O}_8\text{S} + \text{Na}^+$  calcd, 525.1738; found, 525.1747. **15b**:  $^1\text{H}$  NMR (400 MHz,  $\text{CD}_3\text{OD}$ )  $\delta$  8.34 (s, 3H), 8.07 (dd,  $^3J_{\text{H-H}} = 24.0$  Hz,  $^3J_{\text{H-H}} = 7.6$  Hz, 5H), 7.70 (t,  $^3J_{\text{H-H}} = 7.7$  Hz, 1H), 4.33 (dd,  $^3J_{\text{H-H}} = 8.8$  Hz,  $^3J_{\text{H-H}} = 4.7$  Hz, 1H), 3.83–3.49 (m, 16H), 3.43 (s, 3H), 3.34 (t,  $^3J_{\text{H-H}} = 4.7$  Hz, 2H), 3.29–3.33 (m, 1H), 3.18–2.87 (m, 1H).  $^{13}\text{C}$  NMR (75 MHz,  $\text{CD}_3\text{OD}$ )  $\delta$  169.5, 168.4, 142.0, 136.8, 132.5, 131.1, 130.7, 127.6, 71.6, 71.5, 71.3, 71.1, 70.5, 68.2, 54.9, 53.5, 51.7, 42.1, 41.2. HRMS:  $\text{C}_{19}\text{H}_{30}\text{N}_6\text{O}_8\text{S} + \text{H}^+$  calcd, 503.1919; found, 503.1926;  $\text{C}_{19}\text{H}_{30}\text{N}_6\text{O}_8\text{S} + \text{Na}^+$  calcd, 525.1738; found, 525.1739.

**3- and 4-Substituted Methyl-(S)-2-[(2-{2-[2-(2-Azidoethoxy)ethoxy]ethoxy}ethyl)carbamoyl]phenylsulfonamido]-3-[3-[4-(pyrimidin-2-ylamino)piperidin-1-yl]-5-(trifluoromethyl)benzamido]-propanoates (16a,b).** 3-[4-(Pyrimidin-2-ylamino)piperidin-1-yl]-5-(trifluoromethyl)benzoic acid (**3**, 0.38 g, 1.00 mmol) was suspended in DMF (15 mL) and cooled to  $0^\circ\text{C}$ . *N*-Methylmorpholine (NMM, 0.20 g, 1.60 mmol) and (benzotriazol-1-yloxy)tris(dimethylamino)phosphonium hexafluorophosphate (BOP, 0.50 g, 1.10 mmol) were added, and the mixture was stirred for 10 min at  $0^\circ\text{C}$ . The amino derivative (**15a** or **15b**, 0.50 g, 0.94 mmol) was added, and the mixture was stirred at room temperature overnight. After aqueous workup and chromatographic purification (C-18-RP, MeOH/ $\text{H}_2\text{O}$ , 3:2), the products were obtained in 56% (**16a**, 0.45g, 0.53 mmol) and 96% (**16b**, 0.77 g, 0.90 mmol) yield, respectively. **16a**:  $^1\text{H}$  NMR (600 MHz,  $\text{CDCl}_3$ )  $\delta$  8.26 (d,  $^3J_{\text{H-H}} = 4.8$  Hz, 2H), 7.87–7.78 (m, 4H), 7.47 (s, 1H), 7.36 (t,  $^3J_{\text{H-H}} = 6.0$  Hz, 1H, NH), 7.31 (s, 1H), 7.14 (s, 1H), 7.09 (t,  $^3J_{\text{H-H}} = 5.4$  Hz, 1H, NH), 6.50 (t,  $^3J_{\text{H-H}} = 4.8$  Hz, 1H), 5.81 (d,  $^3J_{\text{H-H}} = 7.7$  Hz, 1H, NH), 4.20 (m, 1H), 4.01–3.94 (m, 1H), 3.83–3.73 (m, 2H), 3.66–3.56 (m, 16H), 3.55 (s, 3H), 3.30 (t,  $^3J_{\text{H-H}} = 4.9$  Hz, 2H), 3.02–2.92 (m, 2H), 2.08 (t,  $^3J_{\text{H-H}} = 8.6$  Hz, 2H), 1.60–1.52 (m, 2H).  $^{13}\text{C}$  NMR (151 MHz,  $\text{CDCl}_3$ )  $\delta$  170.1, 167.4, 165.8, 161.4, 158.0, 151.4, 142.3, 138.4, 135.4, 131.6 (q,  $^3J_{\text{C-F}} = 32$  Hz), 127.9, 127.1, 123.9 (q,  $^1J_{\text{C-F}} = 273$  Hz), 117.6, 114.8, 113.2, 110.5, 70.5, 70.4, 70.1, 69.9, 69.5, 55.7, 53.0, 50.6, 47.7, 47.4, 42.5, 40.0, 31.4.  $^{19}\text{F}$ -NMR (564 MHz,  $\text{CDCl}_3$ )  $\delta$  -62.7. HRMS:  $\text{C}_{36}\text{H}_{45}\text{F}_3\text{N}_{10}\text{O}_9\text{S} + \text{H}^+$  calcd, 851.3165; found, 851.3166;  $\text{C}_{36}\text{H}_{45}\text{F}_3\text{N}_{10}\text{O}_9\text{S} + \text{Na}^+$  calcd, 873.2936; found, 873.2964. **16b**:  $^1\text{H}$  NMR (600 MHz,  $\text{DMSO}-d_6$ )  $\delta$  8.24 (d,  $^3J_{\text{H-H}} = 4.7$  Hz, 1H, NH), 8.20 (t,  $^3J_{\text{H-H}} = 1.6$  Hz, 1H), 8.02–7.96 (m, 1H), 7.84 (ddd,  $^3J_{\text{H-H}} = 7.8$  Hz,  $^4J_{\text{H-H}} = 1.8$  Hz,  $^5J_{\text{H-H}} = 1.1$  Hz, 1H), 7.56 (t,  $^3J_{\text{H-H}} = 7.8$  Hz, 1H), 7.50 (s, 1H), 7.35 (s, 1H), 7.28 (s, 1H), 7.09 (d,  $^3J_{\text{H-H}} = 7.9$  Hz, 1H, NH), 6.51 (t,  $^3J_{\text{H-H}} = 4.8$  Hz, 1H), 4.14 (d,  $^3J_{\text{H-H}} = 7.3$  Hz, 1H), 3.96–3.87 (m, 1H), 3.83 (d,  $^3J_{\text{H-H}} = 13.0$  Hz, 2H), 3.56–3.46 (m, 14H), 3.56–3.45 (m, 1H), 3.41 (s, 3H), 3.35–3.32 (m, 1H), 2.99–2.82 (m, 2H), 1.93 (d,  $^3J_{\text{H-H}} = 10.3$  Hz, 2H), 1.55 (dd,  $^3J_{\text{H-H}} = 11.3$  Hz,  $^3J_{\text{H-H}} = 2.7$  Hz, 2H).  $^{13}\text{C}$  NMR (151 MHz,  $\text{DMSO}-d_6$ )  $\delta$  170.5, 166.2, 165.2, 162.1, 158.4, 151.4, 141.5, 136.0, 135.5, 131.3, 130.5 (q,  $^3J_{\text{C-F}} = 32$  Hz), 129.6, 129.3, 125.8, 124.6 (q,  $^1J_{\text{C-F}} = 272$  Hz), 117.6, 113.9, 113.0, 110.4, 70.2, 70.2, 70.1, 70.0, 69.7, 69.2, 55.2, 52.4, 50.4, 47.8, 47.5, 41.8, 36.9, 31.2.  $^{19}\text{F}$ -NMR (564 MHz,  $\text{DMSO}-d_6$ )  $\delta$  -61.6.

HRMS:  $C_{36}H_{45}N_{10}F_3O_9S + H^+$  calcd, 851.3117; found, 851.3103;  $C_{36}H_{45}N_{10}F_3O_9S + Na^+$  calcd, 873.2936; found, 873.2927.

**3- and 4-Substituted (S)-2-[[2-[2-(2-Aminoethoxy)ethoxy]ethoxy]ethyl]carbamoyl]phenylsulfonamido-3-(3-{4-[(1,4,5,6-tetrahydropyrimidin-2-yl)amino]piperidin-1-yl}-5-(trifluoromethyl)benzamido)propanoic Acid (17a,b).** The final precursor amino propanoic acids **17a** and **17b** were obtained after hydrogenolytic reduction and subsequent saponification. In detail, compounds **16a** (0.50 g, 0.59 mmol) and **16b** (0.91 g, 1.10 mmol) were dissolved in methanol/dioxane 1:1 (60–100 mL) containing 1 N HCl (1–2 mL) and platinum dioxide (1% w/w) in a stainless steel autoclave. Hydrogenolytic reduction was accomplished by stirring for 4 h at a hydrogen pressure of 12 atm. After filtration and evaporation, the products were obtained as the monohydrochloride salts in yields of 81% (from **16a**, 397 mg, 480  $\mu$ mol) and 67% (from **16b**, 610 mg, 750  $\mu$ mol), respectively. Subsequent saponification with LiOH (5 equiv) in a THF/MeOH/H<sub>2</sub>O mixture (3:1:1) at room temperature for 5 h yielded the propanoic acids in 75% (**17a**, 291 mg, 357  $\mu$ mol) and 45% (**17b**, 410 mg, 501  $\mu$ mol) yield, respectively, after HPLC purification. **17a**: <sup>1</sup>H NMR (400 MHz, DMSO-*d*<sub>6</sub>)  $\delta$  8.78 (t, <sup>3</sup>J<sub>H-H</sub> = 5.4 Hz, 1H, NH), 8.70 (t, <sup>3</sup>J<sub>H-H</sub> = 5.8 Hz, 1H, NH), 8.46 (d, <sup>3</sup>J<sub>H-H</sub> = 9.2 Hz, 1H, NH), 7.93 (d, <sup>3</sup>J<sub>H-H</sub> = 8.5 Hz, 2H), 7.83 (d, <sup>3</sup>J<sub>H-H</sub> = 8.6 Hz, 2H), 7.64 (d, <sup>3</sup>J<sub>H-H</sub> = 8.2 Hz, 1H, NH), 7.55 (s, 1H), 7.41 (s, 1H), 7.30 (s, 1H), 4.11 (dt, <sup>3</sup>J<sub>H-H</sub> = 8.9 Hz, <sup>3</sup>J<sub>H-H</sub> = 7.0 Hz, 1H), 3.84 (d, <sup>3</sup>J<sub>H-H</sub> = 12.8 Hz, 1H), 3.64–3.46 (m, 13H), 3.45–3.29 (m, 3H), 3.28–3.19 (m, 4H), 2.88 (t, <sup>3</sup>J<sub>H-H</sub> = 11.5 Hz, 2H), 1.91 (d, <sup>3</sup>J<sub>H-H</sub> = 10.4 Hz, 2H), 1.82 (dt, <sup>3</sup>J<sub>H-H</sub> = 11.3 Hz, <sup>3</sup>J<sub>H-H</sub> = 5.8 Hz, 2H), 1.49 (dd, <sup>3</sup>J<sub>H-H</sub> = 20.6 Hz, <sup>3</sup>J<sub>H-H</sub> = 10.6 Hz, 1H). <sup>13</sup>C NMR (101 MHz, DMSO-*d*<sub>6</sub>)  $\delta$  171.0, 165.5, 164.9, 158.4 (q, <sup>3</sup>J<sub>C-F</sub> = 36 Hz), 151.8, 150.7, 143.2, 137.4, 135.7, 130.0, 127.7, 126.4, 124.1 (q, <sup>1</sup>J<sub>C-F</sub> = 273 Hz), 117.3, 113.5, 113.2, 69.6, 69.6, 69.5, 69.5, 68.7, 66.6, 54.8, 47.3, 46.6, 41.5, 39.6, 37.9, 30.8, 19.6. <sup>19</sup>F-NMR (564 MHz, DMSO-*d*<sub>6</sub>)  $\delta$  -61.2. HRMS:  $C_{35}H_{49}F_3N_8O_8S + H^+$  calcd, 815.3355; found, 815.3368. **17b**: <sup>1</sup>H NMR (600 MHz, DMSO-*d*<sub>6</sub>)  $\delta$  8.24 (d, <sup>3</sup>J<sub>H-H</sub> = 4.7 Hz, 1H, NH), 8.20 (t, <sup>3</sup>J<sub>H-H</sub> = 1.6 Hz, 1H), 8.02–7.96 (m, 1H), 7.84 (ddd, <sup>3</sup>J<sub>H-H</sub> = 7.8 Hz, <sup>3</sup>J<sub>H-H</sub> = 1.8 Hz, <sup>5</sup>J<sub>H-H</sub> = 1.1 Hz, 1H), 7.56 (t, <sup>3</sup>J<sub>H-H</sub> = 7.8 Hz, 1H), 7.50 (s, 1H), 7.35 (s, 1H), 7.28 (s, 1H), 7.09 (d, <sup>3</sup>J<sub>H-H</sub> = 7.9 Hz, 1H, NH), 6.57–6.48 (m, 1H), 4.14 (d, <sup>3</sup>J<sub>H-H</sub> = 7.3 Hz, 1H), 3.96–3.87 (m, 1H), 3.83 (d, <sup>3</sup>J<sub>H-H</sub> = 13.0 Hz, 2H), 3.56–3.45 (m, 13H), 3.35–3.32 (m, 4H), 2.99–2.82 (m, 2H), 1.93 (d, <sup>3</sup>J<sub>H-H</sub> = 10.3 Hz, 2H), 1.79 (dd, <sup>3</sup>J<sub>H-H</sub> = 11.4 Hz, <sup>3</sup>J<sub>H-H</sub> = 5.8 Hz, 2H), 1.54–1.45 (m, 2H). <sup>13</sup>C NMR (151 MHz, DMSO-*d*<sub>6</sub>)  $\delta$  171.5, 165.8, 165.2, 162.1, 152.5, 151.6, 141.7, 136.0, 135.4, 131.3, 130.4 (q, <sup>3</sup>J<sub>C-F</sub> = 32 Hz), 129.6, 129.3, 125.8, 124.6 (q, <sup>1</sup>J<sub>C-F</sub> = 272 Hz), 118.2, 113.9, 114.3, 70.2, 70.1, 70.1, 70.0, 69.6, 69.2, 55.2, 47.8, 47.5, 41.5, 38.9, 38.4, 36.9, 31.0, 20.1. <sup>19</sup>F-NMR (282 MHz, DMSO-*d*<sub>6</sub>)  $\delta$  -61.3. HRMS:  $C_{35}H_{49}F_3N_8O_9S + H^+$  calcd, 815.3368; found, 815.3375;  $C_{36}H_{45}F_3N_{10}O_9S + Na^+$  calcd, 837.3188; found, 837.3162.

**Echistatin Assay.** Plates (96 well) were coated with integrin ( $\alpha_v\beta_3$  or  $\alpha_{IIIb}\beta_3$ , 1  $\mu$ g/mL, 100  $\mu$ L) in coating buffer (Tris-HCl 25 mM, NaCl 150 mM, CaCl<sub>2</sub> 1 mM, MgCl<sub>2</sub> 500  $\mu$ M, MnCl<sub>2</sub> 1 mM) at 4 °C overnight. Surfaces were blocked with 1% bovine serum albumin (BSA) in coating buffer for 2 h at rt and washed twice with binding buffer (0.1% BSA, Tris-HCl 25 mM, NaCl 150 mM, CaCl<sub>2</sub> 1 mM, MgCl<sub>2</sub> 500  $\mu$ M, MnCl<sub>2</sub> 1 mM). Antagonists **5**, **17a**, **17b**, and RGD peptide (concentrations from 1 pM to 100  $\mu$ M) and [<sup>125</sup>I]-echistatin (60 pM, PerkinElmer Life Sciences) were added, and incubation was maintained for 3 h at rt. After washing twice with binding buffer, the remaining radioactivity was removed with hot 2 N NaOH (200  $\mu$ L), transferred to counting tubes, and determined with a  $\gamma$ -counter (Wallac Wizard 3, PerkinElmer Life Sciences).

**Fluorescent Labeling of Amino-PEG Derivative.** Amino derivative **17a** was chosen for labeling experiments. An amount of 1.0  $\mu$ mol of **17a** was dissolved in 100  $\mu$ L of DMSO and transferred into 700  $\mu$ L of 0.1 M NaHCO<sub>3</sub> buffer, pH 8.6–9.2. To this solution was added 1.0  $\mu$ mol of dye-NHS ester (DY-495 or Cy 5.5) dissolved in 200  $\mu$ L of DMSO. After shaking for 4–6 h at room temperature, the mixtures were transferred into the HPLC system and purified using the following semipreparative setup: Nucleosil 100-5 C18 column

(250 mm  $\times$  8.0 mm);  $\lambda$  = 254 nm; flow = 5.5 mL/min; eluents: A, water for injection/trifluoroacetic acid (TFA) 1000:1 (v/v); B, acetonitrile/TFA 1000:1 (v/v); DY-495-derivatives were purified as follows: elution gradient: 90% A to 35% A in 15 min, 35% A for 15 min, from 35% to 90% A in 2 min ( $t_R$  = 25.9 min for **17a**–DY-495). The Cy 5.5 derivative was purified as follows: elution gradient: 90% A to 45% A in 15 min, 45% A for 15 min, from 45% to 90% A in 2 min ( $t_R$  = 14.7 min). The desired fractions were collected, and after evaporation of the solvent, the residues were reconstituted in PBS (**17a**–Cy 5.5) or PBS containing 20% DMSO (**17a**–DY-495). The identities of the conjugates were proven by mass spectrometry.

MALDI-MS of **17a**–Cy 5.5:  $C_{76}H_{92}F_3N_{10}O_{22}S_5^+$  calcd  $m/z$ , 1713.5; found  $m/z$ , 1713.4;  $C_{76}H_{92}F_3N_{10}O_{22}S_5Na^+$  calcd  $m/z$ , 1735.5; found  $m/z$ , 1735.4;  $C_{76}H_{90}F_3N_{10}O_{22}S_5Na_2^+$  calcd  $m/z$ , 1757.5; found  $m/z$ , 1757.4.

HRMS of **17a**–DY-495:  $C_{62}H_{71}F_3N_9O_{16}S^+$  calcd  $m/z$ , 1286.4686; found  $m/z$ , 1286.4700;  $C_{62}H_{72}F_3N_9O_{16}S^{2+}$  calcd  $m/z$ , 643.7380; found  $m/z$ , 643.7383.

The concentrations of the tracers were determined by photometric measurements using a Hitachi U-3010 spectrophotometer (Hitachi High-Technologies Europe GmbH, Mannheim, Germany). At least five different concentrations of the reconstituted solutions were measured at wavelengths of 493 nm (**17a**–DY-495) and 676 nm (**17a**–Cy 5.5), respectively. After recording the absorption values, the concentrations were determined employing Lambert–Beer's law (absorption coefficient  $\epsilon_\lambda$  = 70 000 and 250 000 L·mol<sup>-1</sup>·cm<sup>-1</sup> for DY-495 and Cy 5.5, respectively). The determined yields after these steps were 30% (**17a**–DY-495) and 48% (**17a**–Cy 5.5).

**Cell Culture.** Human melanoma M-21 cells,<sup>24</sup> the human adenocarcinoma cell line MCF-7 (ATCC: HTB-22; Manassas, VA), and human glioblastoma U-87MG cells (ATCC: HTB-14; Manassas, VA) were cultured in RPMI-1640 or MEM (Invitrogen Corporation, San Diego, CA) supplemented with 10% fetal calf serum, penicillin, and streptomycin. Cells were grown routinely in a monolayer culture at 37 °C in a 5% CO<sub>2</sub> humidified air atmosphere in T75 cell culture flasks. Medium was changed every 3–4 days. Before use, the cells were incubated with trypsin/EDTA and resuspended in PBS at appropriate concentrations.

**In Vitro Studies on Cells.** Cells (50 000 cells/100  $\mu$ L) were seeded on slides, incubated at 37 °C (5% CO<sub>2</sub>) overnight, washed with PBS, and incubated in fixation solution (4% formalin, rt, 10 min). After washing with PBS, the cells were incubated in blocking solution (PBS/BSA, 0.1%, 15 min, rt), washed twice in PBS (Ca<sup>2+</sup>/Mg<sup>2+</sup>), and preincubated in binding buffer (50 mM NaCl, 10 mM MgCl<sub>2</sub>, 10 mM MnCl<sub>2</sub>, pH 7.2) for 1 min. The cells were incubated with **17a**–DY-495 (0.2 nmol/100  $\mu$ L) at room temperature for 3 h and washed with PBS. Nuclear counterstaining was performed with 4',6'-diamidino-2-phenylindole (DAPI). Fluoromount (Sigma-Aldrich, St. Louis, MO) and cover slides were added. For blocking studies, cells were washed with PBS twice and treated with 0.1  $\mu$ mol of RGD peptide in binding buffer for 10 min. The blocking solution was removed, and 100  $\mu$ L/well of fluorescent tracer **17a**–Cy 5.5 (0.2 nmol/100  $\mu$ L) was added. After an incubation period of 1 h at room temperature, cells were washed again with PBS/Ca<sup>2+</sup>/Mg<sup>2+</sup> and Fluoromount, and cover slides were added. Immunofluorescence was evaluated using fluorescence microscopy (20 $\times$  objective magnification, Nikon TE 2000-S). The microscope was equipped with a mercury vapor lamp, 377/447, 480/535, and 620/775 nm (excitation/emission) filters (DAPI, FITC, and Cy 5.5, respectively), a Nikon DXM1200F camera, and Nikon's NIS-Elements software (Nikon, Tokyo, Japan).

**Xenografts.** All animal experiments were carried out according to approved protocols of the animal ethics committee of the University of Münster, Germany. Athymic 7- to 9-week-old female nude mice were obtained from Charles River (Sulzfeld, Germany) and maintained in a pathogen-free animal facility with food and water available ad libitum. The U-87MG xenografts were established by the subcutaneous injection of 3  $\times$  10<sup>6</sup> viable tumor cells suspended in 200  $\mu$ L of saline into the right hemithorax or the right flank of the animals through 26-gauge needles. Cells were allowed to grow for 8 to 12 days to reach tumor sizes of 4–8 mm.

**In Vivo Fluorescence Reflectance Imaging (FRI).** Near-infrared FRI was performed using the In-Vivo FX Pro Imaging System (Bruker BioSpin GmbH, Rheinstetten, Germany) equipped with a 400 W halogen illuminator with Cy 5.5 bandpass excitation ( $625 \pm 18.0$  nm) and emission filters ( $700 \pm 17.5$  nm). Fluorescence signals were captured with a  $4 \times 10^6$  pixel cooled charge-coupled device (CCD) camera equipped with a 10 $\times$  zoom lens. Mice were anesthetized by isoflurane inhalation and received Cy 5.5-labeled tracer 17a–Cy 5.5 (2.0 nmol/animal,  $n = 3$ –6) dissolved in saline (150  $\mu$ L) via the tail vein. Images were captured at several time points up to 48 h after probe injection, with an acquisition time of 5 s and identical window settings (binning, f-stop, field of view). For biodistribution studies, animals were sacrificed after 24 h (flank xenografts) or 48 h (breast xenografts) by carbon dioxide

inhalation. Organs were removed, washed, and placed on a Petri dish for fluorescence imaging. Fluorescence images were analyzed and coregistered with the anatomic white light images, and region of interest (ROI) analyses were performed using Bruker MI 7.1 software.

**Histological Examination of Tumor Tissue.** After FRI, tumors (breast xenografts) were snap-frozen in cryopreservation medium (OCT) and cryosectioned (5  $\mu$ m). Frozen tissue sections were fixed in methanol for 10 min, air-dried, washed with PBS, and blocked with 10% goat serum/PBS for 20 min. After additional washing, sections were incubated with primary antibody (ab7166, Abcam, Cambridge, UK) at a dilution of 1:100 for 1 h, washed again, and incubated with secondary antibody (FITC-labeled goat anti-mouse 115-095-205, Jackson ImmunoResearch, West Grove, PA) at a dilution of 1:100

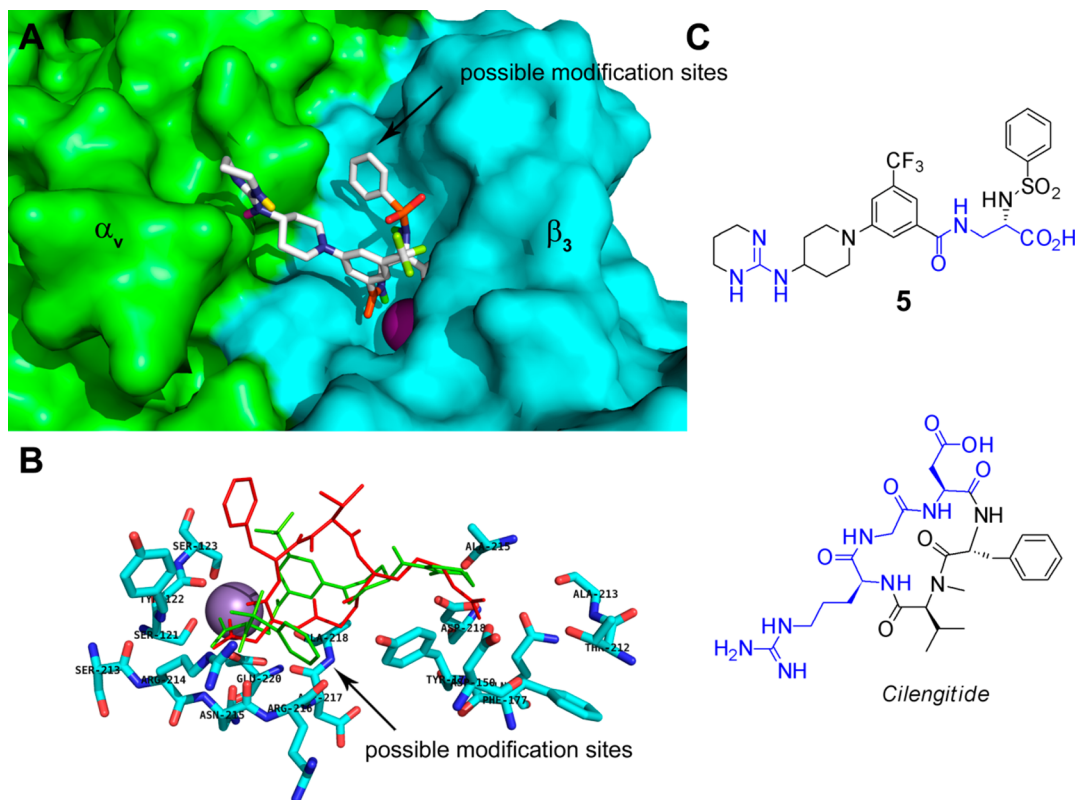
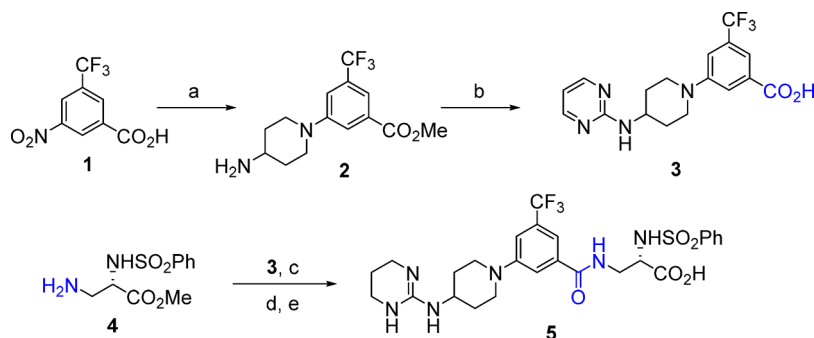


**Figure 1.** (A) Docking results of compound 5 with protein structure 1LSG. (B) Overlay image of the co-crystallized cyclic RGD peptide ciligitide (red) with compound 5 (green) at the MIDAS site of  $\alpha_v\beta_3$  showing the unsubstituted phenyl sulfonamide residue. (C) Molecular structures of lead compound 5 and ciligitide with the important sites displayed in blue.

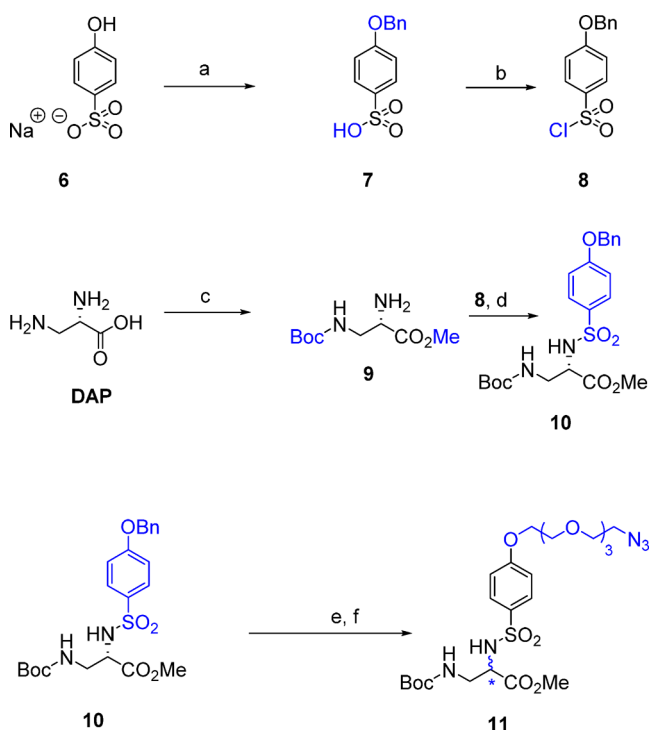
**Scheme 1. Preparation of Lead Compound 5 as Adapted from Kubota<sup>18,a</sup>**



<sup>a</sup>Reactions and conditions: (a) (i)  $\text{SOCl}_2$ , MeOH; (ii) Pd/C,  $\text{H}_2$ , MeOH; (iii) 1,5-dichloropentan-3-one, MeOH, (iv) AcOH,  $\text{H}_2\text{O}$ ; (v)  $\text{BnNH}_2$ ,  $\text{Na}[\text{BH}(\text{AcO})_3]$ ; (vi)  $\text{H}_2$ , Pd(OH)<sub>2</sub>; (b) (i) 2-bromopyrimidine, MeOH; (ii) THF/MeOH/ $\text{H}_2\text{O}$  3:1:1, LiOH (5 equiv); (c) BOP, NMM, DMF; (d) Pd/C,  $\text{H}_2$ , TFA, MeOH; (e) THF/MeOH/ $\text{H}_2\text{O}$  3:1:1, LiOH (5 equiv).

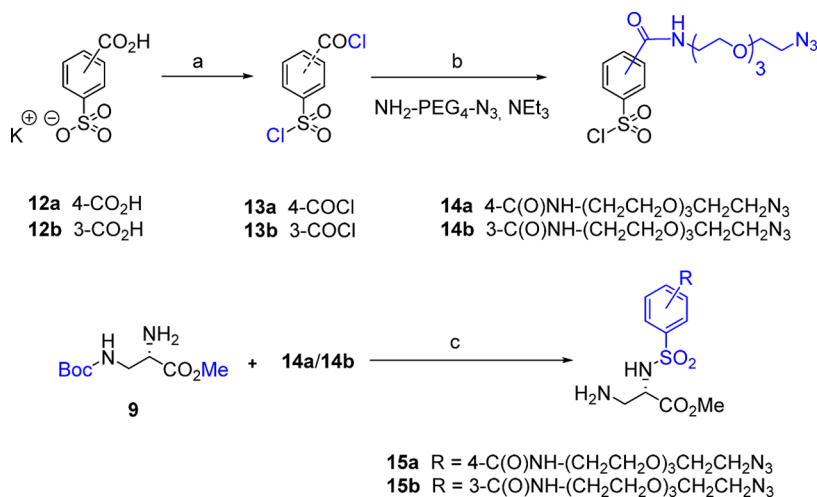
for 1 h. Nuclear counterstain was performed with DAPI. Staining procedures in the absence of the primary antibody served as a control. Slides were washed again with PBS, and Fluoromount and cover slides were added. Tracer binding to tumor tissue was evaluated by incubating fixed sections with 2  $\mu$ M 17a-Cy 5.5 in binding buffer for 1 h at 37 °C. After nuclear counterstaining, slides were washed with PBS, and Fluoromount and cover slides were added. Fluorescence was directly visualized by fluorescence microscopy.

**Scheme 2. Synthesis of Building Block 11 Starting from and *p*-Hydroxybenzenesulfonate 6 and Diaminopropionic Acid (DAP)<sup>a</sup>**



<sup>a</sup>Reactions and conditions: (a) BnBr, NaH, DMF; (b) SOCl<sub>2</sub>, DMF; (c) (i) SOCl<sub>2</sub>, MeOH; (ii) Boc<sub>2</sub>O, Et<sub>3</sub>N, CH<sub>2</sub>Cl<sub>2</sub>; (d) Et<sub>3</sub>N, CH<sub>2</sub>Cl<sub>2</sub>, 0 °C; (e) Pd(OH)<sub>2</sub>, H<sub>2</sub> (40 atm), MeOH/dioxane 1:1; (f) MsO-PEG<sub>4</sub>-N<sub>3</sub>, DMF, Na<sub>2</sub>CO<sub>3</sub>, 90 °C, 16 h.

**Scheme 3. Synthesis of 15a and 15b via PEGylated Arylsulfonyl Chlorides 14a and 14b<sup>a</sup>**



<sup>a</sup>Reactions and conditions: (a) SOCl<sub>2</sub>, DMF; (b) NH<sub>2</sub>-PEG<sub>4</sub>-N<sub>3</sub>, THF, Et<sub>3</sub>N, DMAP, -78 °C; (c) (i) CH<sub>2</sub>Cl<sub>2</sub>, Et<sub>3</sub>N, 0 °C; (ii) 4 M HCl/dioxane, 0 °C.

## RESULTS AND DISCUSSION

The degree of angiogenic activity of tumor lesions is typically closely related to their growth behavior and aggressiveness. One relevant molecular factor determining the angiogenic potential of tumor cells is integrin receptor expression. Particularly in the vasculature, where integrin cell adhesion receptors are highly expressed on proliferating but not on quiescent endothelial cells, integrin activation results in angiogenic sprouting of new vessels and tumor progression. The most common integrin binding sequence, the Arg-Gly-Asp (RGD) motif, has been widely used for endothelial targeting for diagnostic and therapeutic purposes in cancer.<sup>4,6,25</sup> Therapeutic targeting of the  $\alpha_v\beta_3$  integrin has been successfully performed using fusion peptides containing the RGD sequence combined with a truncated tissue factor.<sup>26,27</sup> The cyclic RGD peptide cilengitide,<sup>28,29</sup> a specific  $\alpha_v\beta_3$  integrin antagonist, is currently undergoing clinical trials; this is also true for specific antibodies and a first non-peptide  $\alpha_v\beta_3$  integrin antagonist.<sup>17,30,31</sup> Radiolabeled RGD peptide motifs have been applied as diagnostic agents, demonstrating in vivo target expression by PET.<sup>9,10,14,32,33</sup> More recently, fluorochrome labeling of RGD peptides and tumor targeting with these optical probes using fluorescence reflectance and tomographic imaging methods have been shown to be feasible.<sup>12,13,20,21,34–37</sup> This work aimed at the synthesis and first in vitro and in vivo evaluation of an RGD-mimetic near-infrared fluorescent integrin ligand. Non-peptidic structures offer a number of advantages: they feature wide variability with respect to chemical modifications, e.g., for specificity tuning, options for large-scale syntheses, and high stability. We chose a recently published compound with high affinity and specificity as our lead structure.<sup>18</sup>

**Docking.** To investigate for possible modification sites on the chosen compound, we performed a virtual molecular docking study using the published crystal structure of integrin  $\alpha_v\beta_3$  (PDB code 1LSG) and the free software AutoDock Vina. The co-crystallized RGD ligand cilengitide was removed, and a 3D structure of 5 was inserted. The two different ligands are shown in Figure 1C. Figure 1A shows the location of 5 within the MIDAS binding domain of  $\alpha_v\beta_3$ . The docking results show a bent structure of the molecule at the binding site. In

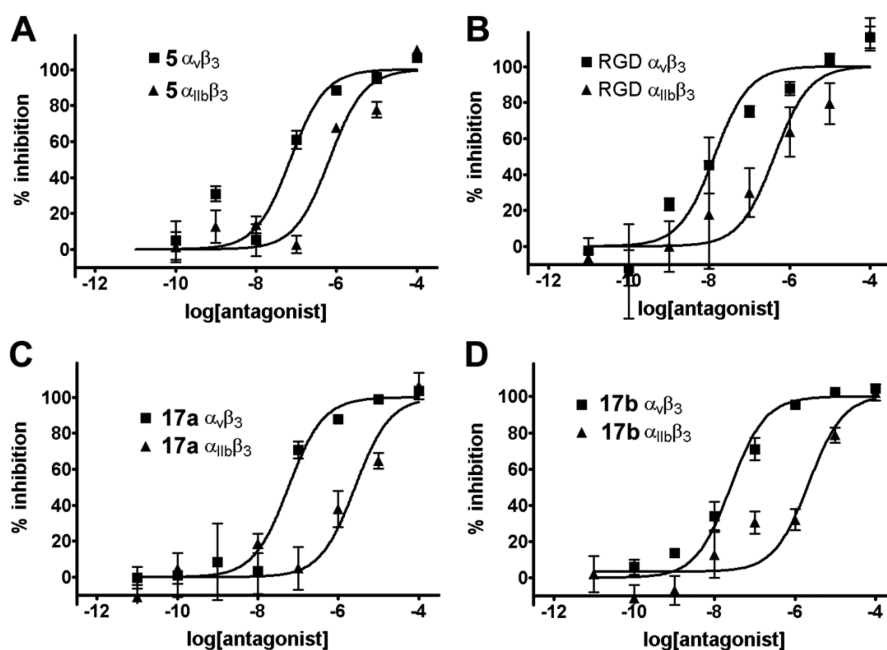
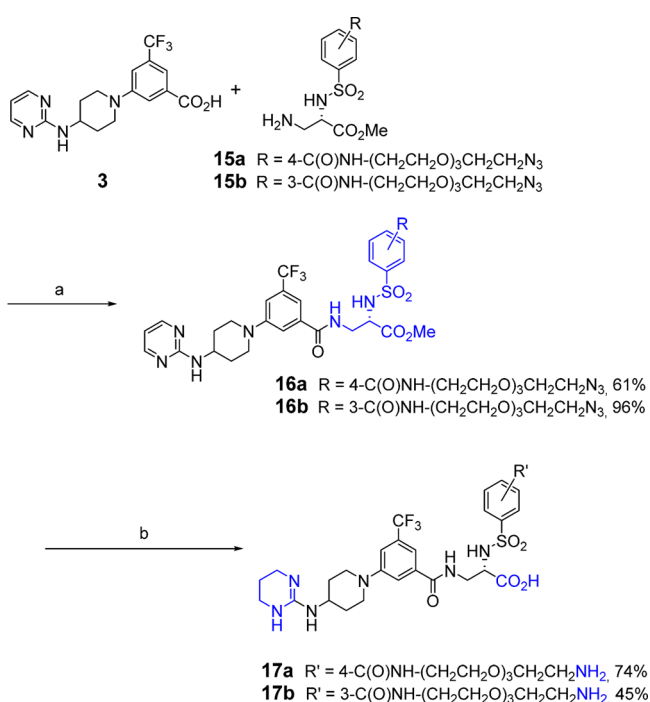


**Figure 2.** Results from competition binding experiments with  $^{125}\text{I}$ -echistatin on  $\alpha_v\beta_3$  and  $\alpha_{IIb}\beta_3$  showing the competition curves of (A) lead compound **5**, (B) a cyclic RGD peptide, and the amino-PEG-derived precursor compounds (C) **17a** and (D) **17b**.

#### Scheme 4. Synthesis of Precursor Compounds **17a** and **17b**<sup>a</sup>



<sup>a</sup>Reactions and conditions: (a) BOP, NMM, DMF 0 °C; (b) (i) PtO<sub>2</sub>, H<sub>2</sub> (12 atm) MeOH, HCl (1 N), (ii) THF/MeOH/H<sub>2</sub>O 3:1:1, LiOH (5 equiv).

comparison to cilengitide (Figure 1B), it is obvious that the two binding moieties (guanidine and carboxylic acid) show similar orientations. Examining for possible modification sites shows that the aromatic sulfonamide side chain is placed inside a small swale that is easily accessible and suggests that a modification at the para or meta position should be possible without compromising the binding affinity. The calculated orientation of **5** is contrary to that of earlier pharmacophore-based

**Table 1**

compound	IC <sub>50</sub> $\alpha_v\beta_3$ (nM)	IC <sub>50</sub> $\alpha_{IIb}\beta_3$ (nM)	specificity
<b>5</b>	77.9 ± 30.7	707 ± 240	1:9
<b>5</b> <sup>a</sup>	18	2000	1:110
<b>17a</b>	58.0 ± 9.7	2800 ± 1050	1:45
<b>17b</b>	25.5 ± 6.0	2340 ± 800	1:88
cyclo-[CRGDC]GK	14.0 ± 4.2	446 ± 157	1:32
cilengitide <sup>b</sup>	0.58	860	1:1500

<sup>a</sup>Kubota et al.<sup>18</sup> <sup>b</sup>Mas-Moruno et al.<sup>29</sup>

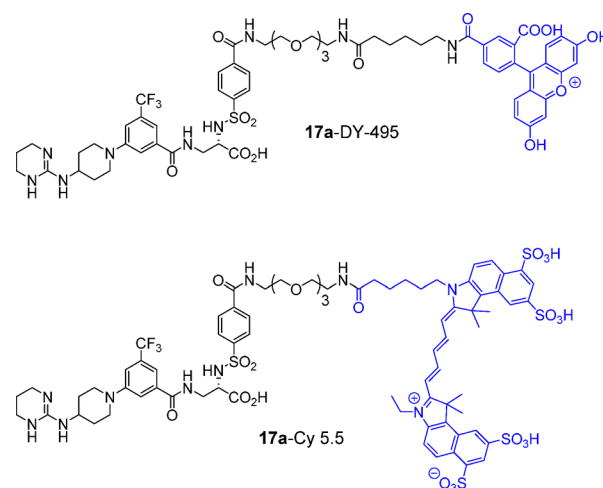


**Figure 3.** Molecular structures of the two synthesized fluorescent tracers for selective  $\alpha_v\beta_3$  imaging. (Top) Fluorescein-derived **17a**–DY-495 can be used for in vitro studies; (Bottom) NIR-dye labeled **17a**–Cy 5.5 is a dedicated tracer for preclinical in vivo imaging.

modeling results, where the Arg-mimetic group often showed different orientations,<sup>38</sup> but it is similar to more recent studies, where more specific compounds were tested.<sup>39–43</sup>

**Chemistry.** The general strategy for the synthesis of lead compound **5** was developed by Kubota et al.<sup>18,44</sup> This synthesis

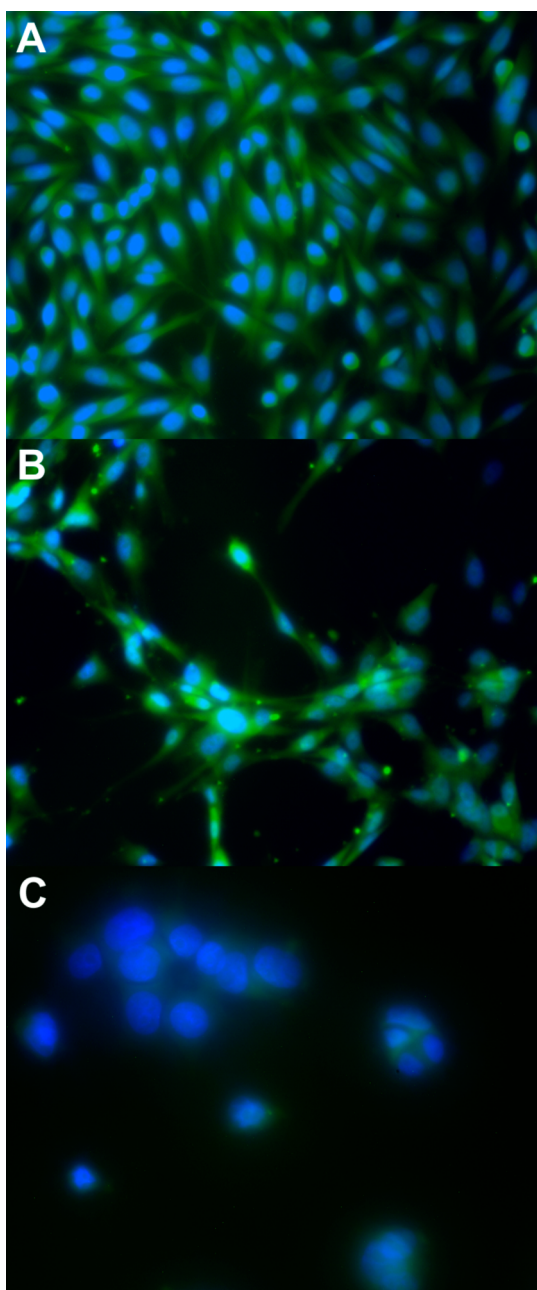


**Figure 4.** In vitro cell binding studies with 17a-DY-495 on (A) M-21 melanoma, (B) U-87MG glioblastoma, and (C) MCF-7 adenocarcinoma cells. Green, tracer fluorescence; blue, DAPI nuclear counterstain.

involved amide coupling of tricyclic aminopyrimidine benzoic acid building block **3** to sulfonamide derivatized aminopropionic acid **4** followed by hydrogenation of the aminopyrimidine moiety and subsequent hydrolysis of the ester group (Scheme 1). In order to assemble the corresponding ligand furnished with a short spacer and an amine functionalization, a mini-PEG chain should be introduced at the phenylsulfonamide residue. The mini-PEG approach has recently been shown to separate dye and ligand sufficiently for preserved receptor affinity.<sup>45,46</sup> Our first approach to modify ligand **5** is outlined in Scheme 2. 4-(Benzyloxy)benzenesulfonyl chloride was synthesized from commercially available sodium-4-hydroxybenzenesulfonate **6** in two steps, as reported by Wang et al.,<sup>47</sup> in 72%

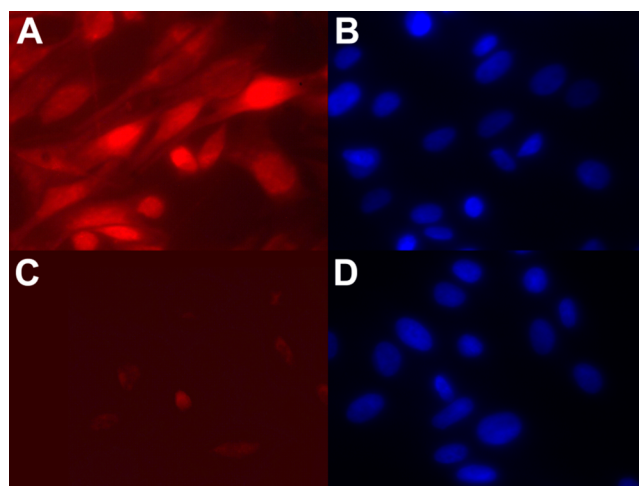


**Figure 5.** In vitro cell binding studies with 17a-Cy 5.5 on M-21 melanoma cells showing the specificity of binding with (C, D) and without (A, B) incubation with an excess of RGD peptide. Red, tracer fluorescence (A, C); blue, DAPI nuclear counterstain (B, D).

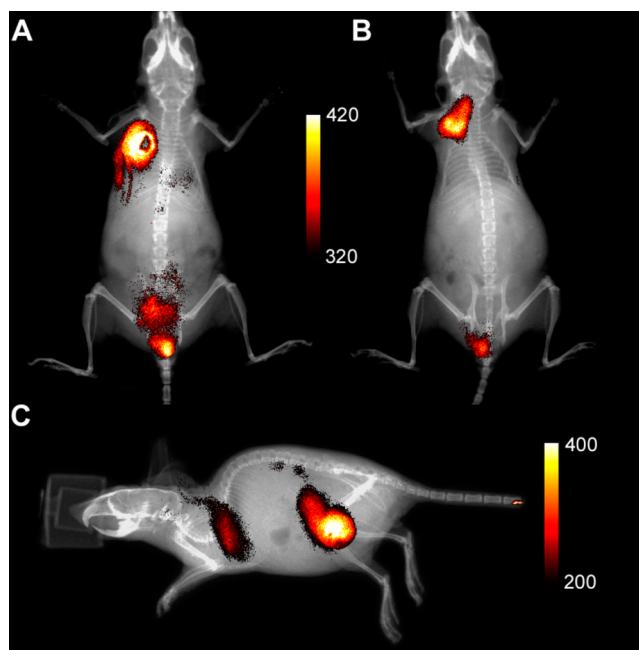


**Figure 6.** Exemplary in vivo overlay images (X-ray/fluorescence) of mice bearing U-87MG xenografts on the (A, B) breast and (C) flank. Animals received 2.0 nmol of 17a-Cy 5.5; images were acquired after 24 h.

overall yield. The resulting arylsulfonyl chloride **8** was coupled with *N*- $\beta$ -Boc-L-2,3-diaminopropionic acid methyl ester **9** to yield compound **10**. After deprotection of the benzyl group (hydrogenolysis), the resulting phenol was coupled with PEG-derivative MsO-PEG<sub>4</sub>-N<sub>3</sub> under basic conditions. Unfortunately, the basic conditions used (relatively high temperatures, strong base) in this step promoted the isomerization of the chiral center in the  $\alpha$  position related to the carbonyl group. Because changing these conditions, such as changing the temperature and leaving group or attempts to PEGylate sodium-4-hydroxybenzenesulfonate **6** directly, offered no significant improvement, we turned our attention to a conceptually different approach based on PEGylated arylsulfonyl chlorides **14a/14b** as building blocks (Scheme 3). This allows

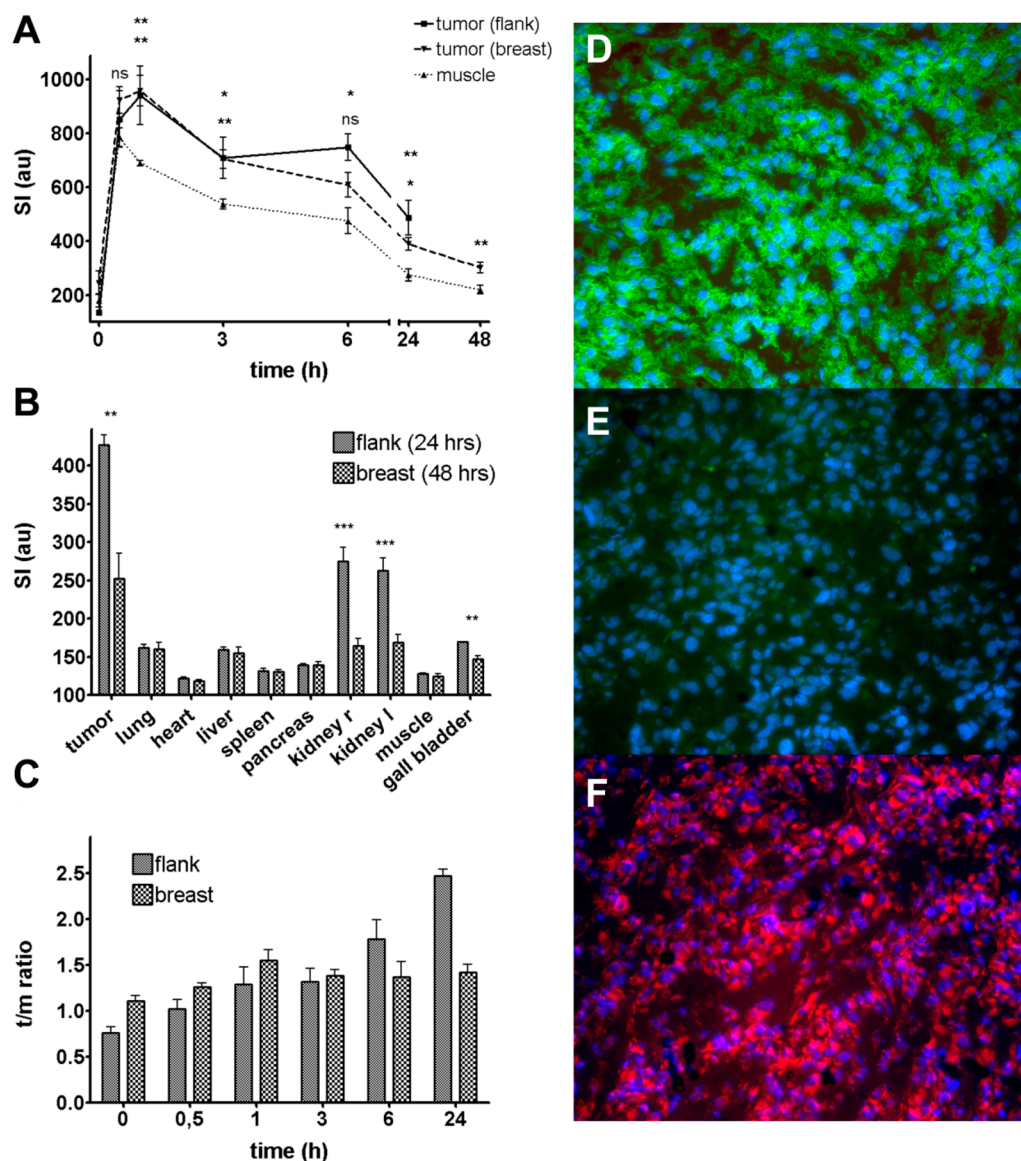


**Figure 7.** Results of in vivo imaging experiments. (A) Fluorescence intensity time curves of tumor xenografts (flank and breast) in comparison to muscle fluorescence. (B) Biodistribution results after 24 h (flank) and 48 h (breast). The fluorescence intensity from selected explanted organs is measured. (C) Comparison of tumor-to-muscle (t/m) ratios of the two xenograft models. Histological examination of target expression in tumor samples (20 $\times$  magnification). (D) The CD51/CD61 antibody demonstrates a high amount of integrin  $\alpha_v\beta_3$  on tumor sections. (E) Control experiment without primary antibody depicting secondary antibody background. (F) Tracer distribution on adjacent tumor sections shows a comparable accumulation at the cell surface (blue, DAPI nuclear counterstain).

coupling under mild conditions with chiral amino acid derivatives like **9**.

The syntheses of key building blocks **15a/15b** were realized by starting from commercially available sulfobenzoic acid monopotassium salts **12a/12b**, which were converted to their corresponding acid chlorides **13a/13b** using thionyl chloride in DMF. The following selective amid coupling with amino PEG derivative  $\text{NH}_2\text{-PEG}_4\text{-N}_3$  was carried out at low temperature ( $-78^\circ\text{C}$ ) in the presence of catalytic amounts of 4-(dimethylamino)pyridine (DMAP) in order to promote the amide formation with carbonyl chloride over sulfochloride function. Furthermore, optimization of the reaction conditions identified THF as the best solvent, giving a yield of up to 72%. *N*-Boc deprotection was carried out by treatment with hydrochloric acid in dioxane to yield building blocks **15a/15b**. In the following step (Scheme 4), tricyclic aminopyrimidine

benzoic acid building block **3** was coupled with **15a/15b** to afford the amides **16a/16b**. Both the azide function and the aminopyrimidine ring were then reduced with hydrogen gas ( $p\text{H}_2 = 12\text{ atm}$ ) and  $\text{PtO}_2$  in a mixture of hydrochloric acid and methanol. Finally, hydrolysis of the ester group with  $\text{LiOH}$  in a  $\text{THF/MeOH/H}_2\text{O}$  solvent system<sup>48</sup> was performed, giving the desired precursor compounds **17a/17b**.

**Competition Binding Assay Using  $^{125}\text{I}$ -Echistatin.** The binding potential of the synthesized precursor compounds **17a** and **17b** was evaluated in a competition binding assay by replacing  $^{125}\text{I}$ -echistatin (Figure 2). The established RGD peptide  $\text{cyclo}[\text{CRGDC}]\text{GK}$  and lead compound **5** were also tested for comparison. All new compounds showed excellent binding to integrin  $\alpha_v\beta_3$ , with  $\text{IC}_{50}$  values in the low nanomolar range, and a good specificity compared to binding to  $\alpha_{\text{IIb}}\beta_3$  (Table 1). The binding of the RGD peptide showed moderate

specificity for  $\alpha_v\beta_3$ , whereas the values we received for compound **5** showed only a low specificity and therefore differed from those found in the literature.

**Cell Binding Studies.** Human melanoma M-21 cells, human adenocarcinoma MCF-7 cells, and human glioblastoma U-87MG cells were tested for target expression by RT-PCR (data not shown), which confirmed described expression patterns.<sup>24,49,50</sup> For in vitro cell binding studies, **17a**-DY-495 and **17a**-Cy 5.5 were used (Figure 3). **17a**-DY-495 shows binding to  $\alpha_v\beta_3$ -positive M-21 melanoma and U-87MG cells (Figure 4A,B) but not to  $\alpha_v\beta_3$ -negative MCF-7 cells (Figure 4C). The binding specificity was evaluated with **17a**-Cy 5.5 on M-21 cells by predosing with excess RGD peptide. The experiment shows that binding of **17a**-Cy 5.5 to M-21 cells was inhibited in the presence of RGD peptide (Figure 5), confirming binding of the tracer to integrin  $\alpha_v\beta_3$ .

**In Vivo Imaging and Target Identification.** We imaged two different U-87MG xenograft models with **17a**-Cy 5.5: one model with tumors on the flank and one with tumors on the breast. Both models showed excellent tracer accumulation at several time points (Figure 6). ROI analysis demonstrated that tumor lesions show an enhancement of signal intensity (SI) between 30 and 60 min, whereas muscle fluorescence is declining (Figure 7A). One hour p.i., both xenografts show highly significant differences between muscle and tumor tissue. This significant difference can mainly be observed throughout the course of the experiment up to 24 or 48 h. Significant differences in SI between the both xenografts were not observed. Tumor-to-muscle (t/m) ratios of breast tumors, however, do not rise above 1.5:1 (measured at 1 h), whereas tumors on the flank show ratios of up to 2.5:1 at 24 h (Figure 7C). The biodistribution of the tracer was examined after 24 h in animals bearing xenografts on the flank and after 48 h in animals bearing xenografts on the breast (Figure 7B). In both cases, SI in tumor tissue was highest, followed by kidneys, liver, lung, and gall bladder. At 24 h, a significantly higher SI was observed in the kidneys and the gall bladder compared to 48 h values. This is probably due to a not yet complete excretion of the tracer at the earlier time point. Also, in tumor tissue, a significant difference in SI was observed, although this might be attributed to the different xenograft location. Histological analysis of tissue sections revealed a high amount of  $\alpha_v\beta_3$  in the tumor xenografts, as identified from specific CD51/CD61 antibody staining (Figure 7D,E). This staining showed similar patterns as those from staining with **17a**-Cy 5.5 (Figure 7F) on adjacent sections, also suggesting the specificity of the developed tracer.

## CONCLUSIONS

In summary, we present here a new non-peptidic fluorescent tracer capable of binding to  $\alpha_v\beta_3$  integrin with high affinity and selectivity with respect to platelet fibrinogen receptor  $\alpha_{IIb}\beta_3$ . The synthesis of the new compound was possible by introducing a PEG-modified arylsulfonyl chloride as the key building block. The in vitro evaluation of the synthesized tracer shows promising results, especially because of the high specificity to the target structure. These favorable characteristics are also reflected in in vivo experiments with murine xenograft models of high  $\alpha_v\beta_3$  integrin expression and will possibly enable a better understanding of integrin pathophysiology.

## AUTHOR INFORMATION

### Corresponding Author

\*Tel: +49 251 8356156. Fax: +49 251 8352067. E-mail: carsten.hoeltke@uni-muenster.de.

### Notes

The authors declare no competing financial interest.

## ACKNOWLEDGMENTS

Financial support by the German Research Foundation (Deutsche Forschungsgemeinschaft, DFG), DFG EI 878/1-1, and Sonderforschungsbereich SFB 656, subprojects A04, B01, C06, and Z05, as well as from the Interdisciplinary Center for Clinical Research (Interdisziplinäres Zentrum für Klinische Forschung, IZKF, Core-Unit PIX) is gratefully acknowledged. The authors wish to thank Ingrid Otto-Valk, Klaudia Niepagenkämper, Vivian Ozurumba, Sandra Höppner, and Ina Winkler for technical assistance.

## ABBREVIATIONS USED

BOP, benzotriazol-1-yloxytris(dimethylamino)phosphonium hexafluorophosphate; CCD, charge-coupled device; DAP, 2,3-diaminopropionic acid; DAPI, 4',6-diamidino-2-phenylindole; FITC, fluorescein isothiocyanate; FRI, fluorescence reflectance imaging; MIDAS, metal ion-dependent adhesion site; NMM, N-methylmorpholine; OCT, optimal cutting temperature; ROI, region of interest; RP, reversed phase; SI, signal intensity; SNR, signal-to-noise ratio

## REFERENCES

- (1) Arnaout, M. A.; Mahalingam, B.; Xiong, J. P. Integrin structure, allostery, and bidirectional signaling. *Annu. Rev. Cell Dev. Biol.* **2005**, *21*, 381–410.
- (2) Goodman, S. L.; Picard, M. Integrins as therapeutic targets. *Trends Pharmacol. Sci.* **2012**, *33*, 405–412.
- (3) Millard, M.; Odde, S.; Neamati, N. Integrin targeted therapeutics. *Theranostics* **2011**, *1*, 154–188.
- (4) Ruoslahti, E.; Pierschbacher, M. D. New perspectives in cell adhesion: RGD and integrins. *Science* **1987**, *238*, 491–497.
- (5) Tucker, G. C. Integrins: molecular targets in cancer therapy. *Curr. Oncol. Rep.* **2006**, *8*, 96–103.
- (6) D'Souza, S. E.; Ginsberg, M. H.; Matsueda, G. R.; Plow, E. F. A discrete sequence in a platelet integrin is involved in ligand recognition. *Nature* **1991**, *350*, 66–68.
- (7) Frishman, W. H.; Burns, B.; Atac, B.; Alturk, N.; Altajar, B.; Lerrick, K. Novel antiplatelet therapies for treatment of patients with ischemic heart disease: inhibitors of the platelet glycoprotein IIb/IIIa integrin receptor. *Am. Heart J.* **1995**, *130*, 877–892.
- (8) Cox, D.; Brennan, M.; Moran, N. Integrins as therapeutic targets: lessons and opportunities. *Nat. Rev. Drug Discovery* **2010**, *9*, 804–820.
- (9) Beer, A. J.; Kessler, H.; Wester, H. J.; Schwaiger, M. PET imaging of integrin  $\alpha_v\beta_3$  expression. *Theranostics* **2011**, *1*, 48–57.
- (10) Beer, A. J.; Pelisek, J.; Heider, P.; Saraste, A.; Reeps, C.; Metz, S.; Seidl, S.; Kessler, H.; Wester, H. J.; Eckstein, H. H.; Schwaiger, M. PET/CT imaging of integrin  $\alpha_v\beta_3$  expression in human carotid atherosclerosis. *J. Am. Coll. Cardiol., Cardiovasc. Imaging* **2014**, *7*, 178–187.
- (11) Cai, W.; Niu, G.; Chen, X. Imaging of integrins as biomarkers for tumor angiogenesis. *Curr. Pharm. Des* **2008**, *14*, 2943–2973.
- (12) Trajkovic-Arsic, M.; Mohajerani, P.; Sarantopoulos, A.; Kalideris, E.; Steiger, K.; Esposito, I.; Ma, X.; Themelis, G.; Burton, N.; Michalski, C. W.; Kleeff, J.; Stangl, S.; Beer, A. J.; Pohle, K.; Wester, H. J.; Schmid, R. M.; Braren, R.; Ntziachristos, V.; Sivek, J. T. Multimodal molecular imaging of integrin  $\alpha_v\beta_3$  for in vivo detection of pancreatic cancer. *J. Nucl. Med.* **2014**, *55*, 446–451.

- (13) Ye, Y.; Chen, X. Integrin targeting for tumor optical imaging. *Theranostics* **2011**, *1*, 102–126.
- (14) Gärtner, F. C.; Kessler, H.; Wester, H. J.; Schwaiger, M.; Beer, A. J. Radiolabelled RGD peptides for imaging and therapy. *Eur. J. Nucl. Med. Mol. Imaging* **2012**, *39*, S126–138.
- (15) Bledzka, K.; Smyth, S. S.; Plow, E. F. Integrin  $\alpha$ IIb $\beta$ 3: from discovery to efficacious therapeutic target. *Circ. Res.* **2013**, *112*, 1189–1200.
- (16) Uyarel, H.; Uzunlar, B.; Unal Dayi, S.; Tartan, Z.; Samur, H.; Kasikcioglu, H.; Akgul, O.; Simsek, D.; Erdem, I.; Okmen, E.; Cam, N. Effect of tirofiban therapy on ST segment resolution and clinical outcomes in patients with ST segment elevated acute myocardial infarction undergoing primary angioplasty. *Cardiology* **2006**, *105*, 168–175.
- (17) Rosenthal, M. A.; Davidson, P.; Rolland, F.; Campone, M.; Xue, L.; Han, T. H.; Mehta, A.; Berd, Y.; He, W.; Lombardi, A. Evaluation of the safety, pharmacokinetics and treatment effects of an  $\alpha$ V $\beta$ 3 integrin inhibitor on bone turnover and disease activity in men with hormone-refractory prostate cancer and bone metastases. *Asia Pac. J. Clin. Oncol.* **2010**, *6*, 42–48.
- (18) Kubota, D.; Ishikawa, M.; Yahata, N.; Murakami, S.; Fujishima, K.; Kitakaze, M.; Ajito, K. Tricyclic pharmacophore-based molecules as novel integrin  $\alpha$ V $\beta$ 3 antagonists. Part IV: preliminary control of  $\alpha$ V $\beta$ 3 selectivity by meta-oriented substitution. *Bioorg. Med. Chem.* **2006**, *14*, 4158–4181.
- (19) Tahtaoui, C.; Parrot, I.; Klotz, P.; Guillier, F.; Galzi, J. L.; Hibert, M.; Ilien, B. Fluorescent pirenzepine derivatives as potential bitopic ligands of the human M1 muscarinic receptor. *J. Med. Chem.* **2004**, *47*, 4300–4315.
- (20) von Wallbrunn, A.; Hölte, C.; Zühlendorf, M.; Heindel, W.; Schäfers, M.; Bremer, C. In vivo imaging of integrin  $\alpha$ V $\beta$ 3 expression using fluorescence-mediated tomography. *Eur. J. Nucl. Med. Mol. Imaging* **2007**, *34*, 745–754.
- (21) Waldeck, J.; Häger, F.; Hölte, C.; Lanckohr, C.; von Wallbrunn, A.; Torsello, G.; Heindel, W.; Theilmeier, G.; Schäfers, M.; Bremer, C. Fluorescence reflectance imaging of macrophage-rich atherosclerotic plaques using an  $\alpha$ V $\beta$ 3 integrin-targeted fluorochrome. *J. Nucl. Med.* **2008**, *49*, 1845–1851.
- (22) Trott, O.; Olson, A. J. AutoDock Vina: improving the speed and accuracy of docking with a new scoring function, efficient optimization, and multithreading. *J. Comput. Chem.* **2010**, *31*, 455–461.
- (23) Liu, J.; Zhou, Y.; Wu, Y.; Li, X.; Chan, A. S. C. Asymmetric transfer hydrogenation of ketones with a polyethylene glycol bound Ru catalyst in water. *Tetrahedron: Asymmetry* **2008**, *19*, 832–837.
- (24) Felding-Habermann, B.; Mueller, B. M.; Romerdahl, C. A.; Cheresch, D. A. Involvement of integrin  $\alpha$ V gene expression in human melanoma tumorigenicity. *J. Clin. Invest.* **1992**, *89*, 2018–2022.
- (25) Cheresch, D. A.; Spiro, R. C. Biosynthetic and functional properties of an Arg-Gly-Asp-directed receptor involved in human melanoma cell attachment to vitronectin, fibrinogen, and von Willebrand factor. *J. Biol. Chem.* **1987**, *262*, 17703–17711.
- (26) Kessler, T.; Bieker, R.; Padro, T.; Schwöppe, C.; Persigehl, T.; Bremer, C.; Kreuter, M.; Berdel, W. E.; Mesters, R. M. Inhibition of tumor growth by RGD peptide-directed delivery of truncated tissue factor to the tumor vasculature. *Clin. Cancer Res.* **2005**, *11*, 6317–6324.
- (27) Kessler, T.; Schwöppe, C.; Liersch, R.; Schliemann, C.; Hintelmann, H.; Bieker, R.; Berdel, W. E.; Mesters, R. M. Generation of fusion proteins for selective occlusion of tumor vessels. *Curr. Drug Discovery Technol.* **2008**, *5*, 1–8.
- (28) Dechantsreiter, M. A.; Planker, E.; Mathä, B.; Lohof, E.; Hölzemann, G.; Jonczyk, A.; Goodman, S. L.; Kessler, H. N-Methylated cyclic RGD peptides as highly active and selective  $\alpha$ V $\beta$ 3 integrin antagonists. *J. Med. Chem.* **1999**, *42*, 3033–3040.
- (29) Mas-Moruno, C.; Rechenmacher, F.; Kessler, H. Cilengitide: the first anti-angiogenic small molecule drug candidate design, synthesis and clinical evaluation. *Anticancer Agents Med. Chem.* **2010**, *10*, 753–768.
- (30) Wirth, M.; Heidenreich, A.; Gschwend, J. E.; Gil, T.; Zastrow, S.; Laniado, M.; Gerloff, J.; Zühlendorf, M.; Mordenti, G.; Uhl, W.; Lannert, H. A multicenter phase I study of EMD 525797 (DI17E6), a novel humanized monoclonal antibody targeting  $\alpha$ V integrins, in progressive castration-resistant prostate cancer with bone metastases after chemotherapy. *Eur. Urol.* **2014**, *65*, 897–904.
- (31) Alva, A.; Slovin, S.; Daignault, S.; Carducci, M.; Dipaola, R.; Pienta, K.; Agus, D.; Cooney, K.; Chen, A.; Smith, D. C.; Hussain, M. Phase II study of cilengitide (EMD 121974, NSC 707544) in patients with non-metastatic castration resistant prostate cancer, NCI-6735. A study by the DOD/PCF prostate cancer clinical trials consortium. *Invest. New Drugs* **2012**, *30*, 749–757.
- (32) Dearing, J. L.; Barnes, J. W.; Panigrahy, D.; Zimmerman, R. E.; Fahey, F.; Treves, S. T.; Morrison, M. S.; Kieran, M. W.; Packard, A. B. Specific uptake of [<sup>99m</sup>Tc]NC100692, an  $\alpha$ V $\beta$ 3-targeted imaging probe, in subcutaneous and orthotopic tumors. *Nucl. Med. Biol.* **2013**, *40*, 788–794.
- (33) Israel, I.; Richter, D.; Stritzker, J.; van Ooschot, M.; Donat, U.; Buck, A. K.; Samnick, S. PET imaging with [<sup>68</sup>Ga]NOTA-RGD for prostate cancer: a comparative study with [<sup>18</sup>F]fluorodeoxyglucose and [<sup>18</sup>F]fluoroethylcholine. *Curr. Cancer Drug Targets* **2014**, *14*, 371–379.
- (34) Lanzardo, S.; Conti, L.; Brioschi, C.; Bartolomeo, M. P.; Arosio, D.; Belvisi, L.; Manzoni, L.; Maiocchi, A.; Maisano, F.; Forni, G. A new optical imaging probe targeting  $\alpha$ V $\beta$ 3 integrin in glioblastoma xenografts. *Contrast Media Mol. Imaging* **2011**, *6*, 449–458.
- (35) Cao, J.; Wan, S.; Tian, J.; Li, S.; Deng, D.; Qian, Z.; Gu, Y. Fast clearing RGD-based near-infrared fluorescent probes for in vivo tumor diagnosis. *Contrast Media Mol. Imaging* **2012**, *7*, 390–402.
- (36) Cheng, Z.; Wu, Y.; Xiong, Z.; Gambhir, S. S.; Chen, X. Near-infrared fluorescent RGD peptides for optical imaging of integrin  $\alpha$ V $\beta$ 3 expression in living mice. *Bioconjugate Chem.* **2005**, *16*, 1433–1441.
- (37) Mathejczyk, J. E.; Pauli, J.; Dullin, C.; Napp, J.; Tietze, L. F.; Kessler, H.; Resch-Genger, U.; Alves, F. Spectroscopically well-characterized RGD optical probe as a prerequisite for lifetime-gated tumor imaging. *Mol. Imaging* **2011**, *10*, 469–480.
- (38) Dayam, R.; Aiello, F.; Deng, J.; Wu, Y.; Garofalo, A.; Chen, X.; Neamati, N. Discovery of small molecule integrin  $\alpha$ V $\beta$ 3 antagonists as novel anticancer agents. *J. Med. Chem.* **2006**, *49*, 4526–4534.
- (39) Bochen, A.; Marelli, U. K.; Otto, E.; Pallarola, D.; Mas-Moruno, C.; Di Leva, F. S.; Boehm, H.; Spatz, J. P.; Novellino, E.; Kessler, H.; Marinelli, L. Biselectivity of isoDGR peptides for fibronectin binding integrin subtypes  $\alpha$ 5 $\beta$ 1 and  $\alpha$ v $\beta$ 6: conformational control through flanking amino acids. *J. Med. Chem.* **2013**, *56*, 1509–1519.
- (40) Neubauer, S.; Rechenmacher, F.; Brimioulle, R.; Di Leva, F. S.; Bochen, A.; Sobahi, T. R.; Schottelius, M.; Novellino, E.; Mas-Moruno, C.; Marinelli, L.; Kessler, H. Pharmacophoric modifications lead to superpotent  $\alpha$ v $\beta$ 3 integrin ligands with suppressed  $\alpha$ S $\beta$ 1 activity. *J. Med. Chem.* **2014**, *57*, 3410–3417.
- (41) Heckmann, D.; Meyer, A.; Laufer, B.; Zahn, G.; Stragies, R.; Kessler, H. Rational design of highly active and selective ligands for the  $\alpha$ S $\beta$ 1 integrin receptor. *ChemBioChem* **2008**, *9*, 1397–1407.
- (42) Neubauer, S.; Rechenmacher, F.; Beer, A. J.; Curnis, F.; Pohle, K.; D'Alessandria, C.; Wester, H. J.; Reuning, U.; Corti, A.; Schwaiger, M.; Kessler, H. Selective imaging of the angiogenic relevant integrins  $\alpha$ S $\beta$ 1 and  $\alpha$ V $\beta$ 3. *Angew. Chem., Int. Ed.* **2013**, *52*, 11656–11659.
- (43) Rechenmacher, F.; Neubauer, S.; Polleux, J.; Mas-Moruno, C.; De Simone, M.; Cavalcanti-Adam, E. A.; Spatz, J. P.; Fassler, R.; Kessler, H. Functionalizing  $\alpha$ V $\beta$ 3- or  $\alpha$ S $\beta$ 1-selective integrin antagonists for surface coating: a method to discriminate integrin subtypes in vitro. *Angew. Chem., Int. Ed.* **2013**, *52*, 1572–1575.
- (44) Kubota, D.; Ishikawa, M.; Yamamoto, M.; Murakami, S.; Hachisu, M.; Katano, K.; Ajito, K. Tricyclic pharmacophore-based molecules as novel integrin  $\alpha$ (v) $\beta$ 3 antagonists. Part 1: design and synthesis of a lead compound exhibiting  $\alpha$ V $\beta$ 3/ $\alpha$ IIb $\beta$ 3 dual antagonistic activity. *Bioorg. Med. Chem.* **2006**, *14*, 2089–2108.

(45) Faust, A.; Waschkau, B.; Waldeck, J.; Höltnke, C.; Breyholz, H. J.; Wagner, S.; Kopka, K.; Heindel, W.; Schäfers, M.; Bremer, C. Synthesis and evaluation of a novel fluorescent photoprobe for imaging matrix metalloproteinases. *Bioconjugate Chem.* **2008**, *19*, 1001–1008.

(46) Faust, A.; Waschkau, B.; Waldeck, J.; Höltnke, C.; Breyholz, H. J.; Wagner, S.; Kopka, K.; Schober, O.; Heindel, W.; Schäfers, M.; Bremer, C. Synthesis and evaluation of a novel hydroxamate based fluorescent photoprobe for imaging of matrix metalloproteinases. *Bioconjugate Chem.* **2009**, *20*, 904–912.

(47) Wang, M.; Gao, M. Z.; Miller, K. D.; Sledge, G. W.; Hutchins, G. D.; Zheng, Q. H. Synthesis of new carbon-11-labeled 7-aryl-aminindoline-1-sulfonamides as potential PET agents for imaging of tubulin polymerization in cancers. *J. Labelled Compd. Radiopharm.* **2008**, *51*, 6–11.

(48) Corey, E. J.; Su, W. G. A stereospecific synthesis of a dihydrofuran analog of leukotriene-A4. *Tetrahedron Lett.* **1990**, *31*, 2089–2092.

(49) Rutka, J. T.; Muller, M.; Hubbard, S. L.; Forsdike, J.; Dirks, P. B.; Jung, S.; Tsugu, A.; Ivanchuk, S.; Costello, P.; Mondal, S.; Ackerley, C.; Becker, L. E. Astrocytoma adhesion to extracellular matrix: functional significance of integrin and focal adhesion kinase expression. *J. Neuropathol. Exp. Neurol.* **1999**, *58*, 198–209.

(50) Taherian, A.; Li, X.; Liu, Y.; Haas, T. A. Differences in integrin expression and signaling within human breast cancer cells. *BMC Cancer* **2011**, *11*, 293.